Effect of temperature on convective-reactive transport of CO2 in geological formations

Sara Tabrizinejadas, Marwan Fahs, Hussein Hoteit, Anis Younes, Behzad Ataie-Ashtiani, Craig Simmons, Jerome Carrayrou

To cite this version:

Sara Tabrizinejadas, Marwan Fahs, Hussein Hoteit, Anis Younes, Behzad Ataie-Ashtiani, et al.. Effect of temperature on convective-reactive transport of CO2 in geological formations. International Journal of Greenhouse Gas Control, 2023, 128, pp.103944. 10.1016/j.ijggc.2023.103944 . hal-04296438

HAL Id: hal-04296438
https://hal.science/hal-04296438v1

Submitted on 23 Nov 2023

Effect of temperature on convective-reactive transport of CO_2 in geological formations

Sara Tabrizinejadas[a], *Marwan Fahs*[a], *Hussein Hoteit*[b], *Anis Younes*[a], *Behzad Ataie-Ashtiani*[c]
Craig T. Simmons[c], *Jerome Carrayrou*[a]

[a] Institut Terre et Environnement de Strasbourg, Université de Strasbourg, CNRS, ENGEES, UMR 7063, Strasbourg, France

[b]Physical Science and Engineering Division, King Abdullah University of Science and Technology (KAUST), Thuwal, Saudi Arabia

[c]National Centre for Groundwater Research and Training and College of Science and Engineering, Flinders University, Adelaide, South Australia, Australia

Submitted to *International journal of Greenhouse gas control*

Abstract

Geological CO_2 sequestration (GCS) remains the main promising solution to mitigate global warming. Understating the fate of CO_2 behavior is crucial for securing its containment in the reservoir and predicting the impact of dissolved CO_2 on the host formation. Most modeling-based studies in the literature investigated the convective-reactive transport of CO_2 by assuming isothermal conditions. The effect of temperature on the convective-reactive transport of CO_2 is still poorly understood, particularly at the field scale. The objective of this study is to provide an in-depth understanding of CO_2-related reactive thermohaline convection (RTHC) processes at field scale. Thus, a new numerical model based on advanced finite element formulations is developed. The new model incorporates an accurate time integration scheme with error control. Numerical experiments confirm high accuracy and efficiency of the newly developed model. The effect of temperature on CO_2 transport is investigated for a field case in the Viking reservoir in the North Sea. Results show that including the temperature effect intensifies the fingering processes and, consequently, CO_2 dissolution. Neglecting the thermal convection processes and the impact of temperature on the dissolution rate can significantly impact the model predictions. A sensitivity analysis is developed to understand the effect of parameters governing the dissolution rate on the fingering phenomenon and the total CO_2 flux.

Keywords: CO_2 geological sequestration; Thermohaline convective processes; dissolution; Arrhenius law; advanced finite element methods; field case application;

1. Introduction

Global warming is a crucial aspect of climate change, causing a wide range of consequences such as an increase in the frequency and severity of adverse weather events (Chen et al., 2021; Collins et al., 2013; Shi et al., 2020), an increase in global temperature at $1.5^{\circ}C$ above the preindustrial level (Masson-Delmotte et al., 2018), ramifications in ecosystems such as desertification in arid and semi-arid regions (Chen et al., 2021; Wang et al., 2009) and reduction in bio-diversity ("IPCC. (2019).," n.d.). Global warming is mainly related to anthropogenic greenhouse gas emissions. Burning fossil fuels (coal, oil, and gas), as primary energy sources, and large-scale deforestation have led to an accumulation of large amounts of greenhouse gases in the atmosphere, of which the most important is carbon dioxide (CO_2). Despite the ongoing efforts on reducing the use of fossil fuels as the source of energy and substituting renewable sources, currently, most of the worldwide power plants are based on fossil fuels (Whitley, 2018). Therefore, the emission of CO_2 to the atmosphere is currently inevitable and until other inexpensive, clean, and plentiful technologies are available, a temporary possible way to deal with global warming is mitigating the existing CO_2 in the atmosphere. To this end, various approaches have been suggested including geologic CO_2 sequestration (GCS), which is the most effective technology to mitigate large-scale CO_2 emissions in the atmosphere (Zhang and Huisingh, 2017). In the Paris agreement, this approach is introduced as one of the most promising solutions to address the global warming challenge (UNFCCC, 2015).

GCS consists of capturing CO_2 emissions at the industrial combustion sources (mainly fossil fuel-based power plants), compressing it to its supercritical state, transporting it, and injecting the supercritical CO_2 into deep saline aquifers or depleted oil or gas reservoirs for long-term storage. GCS involves a complex series of technologies based on the knowledge of geology, in-situ fluid chemistry, geochemistry, hydrology, and environmental science. Despite the reliability and richness of the injection techniques (Hoteit et al., 2019), the long-term geological storage capacity of CO_2 is not fully understood.

Understating the fate of CO_2 in the geological formation is essential for securing the sequestration and predicting the impact of dissolved CO_2 on host formation. In this context, numerical modeling has become an essential tool that is widely used for several field applications such as understanding physical processes, predicting the storage capacity, evaluating leakage risks, and designing storage systems (Emami-Meybodi et al., 2015; Jiang, 2011; Nordbotten and Celia, 2011). Despite the significant effort made in recent years on numerical modeling of GCS, some challenges are yet to be resolved. For instance, the robustness, reliability, accuracy, and large-scale applicability of these numerical models are not fully understood. Research on the development of new numerical models is indispensable to improve the capacity of current simulators and to include further functionalities related to new applications.

The injected CO_2 can be trapped through various physical and chemical mechanisms. This covers stratigraphic, residual, solubility, and mineral trappings (Kim et al., 2019). Physical or stratigraphic trapping is a crucial mechanism to ensure long-term entrapment of CO_2. Due to the low density of CO_2 compared to the brine in saline aquifers, injected CO_2 migrates upward in the formation until reaching an impermeable cap rock where it is physically entrapped, forming a gas cap. CO_2 continues to dissolve in brine, leading to solubility trapping. For large time scales, CO_2 can also chemically interact with rock formation. The dissolution of CO_2 in water increases its acidity, causing several primary minerals of the host rocks to dissolve into the formation water. As a result, the concentration of some cations such as Ca^{2+}, Mg^{2+}, and Fe^{2+} increases. Reactions between these cations and carbonic acid can form carbonate minerals such as $CaCO_3$, $MgCO_3$, and $FeCO_3$. This interaction is defined as mineral trapping (Zhang and Song, 2014), (Soltanian et al., 2019). In this work, we focus on solubility and mineral trappings which are crucial trapping processes due to their highly secure storage characteristics (Soltanian et al., 2017). In the following sections, we discuss two main shortcomings of the current numerical models and existing modeling-based studies.

The first challenge of numerical models is their capacity to reproduce the multi-physical processes at the interface between the structurally trapped CO_2 and the brine. Indeed, at this interface, CO_2 dissolution in the brine occurs due to mixing processes, where a CO_2-laden brine is formed whose density is higher than the underlying brine. This results in additional dissolution related to gravity-induced fingering, caused by the convective flow (Lu et al., 2009). The effect of convective flow on CO_2 dissolution at the field scale has been discussed by Sathaye et al. (2014) and Ahmadinia et al. (2020) (Ahmadinia et al., 2020; Sathaye et al., 2014). Several modeling-based studies investigated the solubility trapping of CO_2 with the variable-density flow model coupling groundwater flow and mass transport under variable fluid density conditions. Depending on the objective of the study, different assumptions have been considered regarding the various physical processes. Several studies addressed the non-reactive convective flow (Farajzadeh et al., 2011; Hamann et al., 2015; Hewitt et al., 2014; Hidalgo and Carrera, 2009; Riaz et al., 2006; Singh and Islam, 2018). Convective-reactive CO_2 dissolution is extensively investigated in the literature (e.g., (Andres and Cardoso, 2011; Emami-Meybodi et al., 2015; Ghesmat et al., 2011; Ghoshal et al., 2017; Hidalgo et al., 2015; Kim et al., 2019; Shafabakhsh et al., 2021). For instance, Babaei and Islam (2018) (Babaei and Islam, 2018) investigated convective-reactive CO_2 dissolution in aquifers with an immobile water zone, while Erfani et al. (2020) (Erfani et al., 2020) studied the effect of geochemical reactions on CO_2 dissolution in sandstone aquifers. Most previous works assume isothermal conditions. However, it is well-known that temperature gradient, naturally in a reservoir or artificially introduced by CO_2 injection, can affect gravitational instability, fluid properties (notably viscosity), and dissolution processes (Ahmadinia et al., 2020; Emami-Meybodi et al., 2015).

The coupled thermal and solute convection is usually called double diffusion convection or thermohaline convection (THC). Specific interests in THC of CO_2 appeared recently due to new applications involving coupled carbon storage and geothermal extraction (Wu and Li, 2020). Islam et al. (2013, 2014a) (A. W. Islam et al., 2014; Islam et al., 2013a), investigated THC of CO_2 in a brine-saturated geothermal reservoir. However, reactive THC (RTHC) of CO2 is not well investigated in the literature (A. Islam et al., 2014), and the effect of temperature on convective-reactive CO_2 dissolution are still poorly understood (Boudreau et al., 2020; Sjöberg and Rickard, 1984).

While broad interest has been paid to the numerical solutions of the equations governing reactive processes, the equations describing transport and flow processes are usually solved based on standard finite element (FE) or finite volume methods. For instance, Babaei and Islam (2018) (Babaei and Islam, 2018) solved the stream function form of the governing equations using finite difference methods. The standard FE method is used in Kim et al. (2019) (Kim et al., 2019). The finite volume method is used in Farajzadeh et al. (2011) (Farajzadeh et al., 2011). A survey review on the numerical schemes used in the simulations of convective dissolution of CO_2 is reported in Emami-Meybodi et al. (2015) (Emami-Meybodi et al., 2015). The standard numerical schemes used in the existing codes limit the applicability and reliability of these codes for the simulation of GCS at large space and time scales. Several works have shown that numerical simulations of variable-density flow problems are highly sensitive to the numerical scheme used in the approximation of the governing equations (Prasad and Simmons, 2005; van Reeuwijk et al., 2009; Voss et al., 2010). Standard FE or finite volume methods may generate unphysical oscillations that can affect the solutions' accuracy and convergence of the nonlinear solvers (Koohbor et al., 2020; Miller et al., 2013). Upwind schemes are usually implemented to avoid spurious oscillations ((Miller et al., 2013) and references therein). These schemes can reduce the numerical instability but at the expense of introducing numerical diffusion that can overestimate the mixing processes of CO_2. Numerical diffusion can also overestimate the dissolution processes (Batlle et al., 2002). This can affect the predictions of domain clogging due to chemical reactions (Xu et al., 2017). In addition, in existing codes, reactive processes are usually included via the operator splitting approach. For kinetic reactions, this approach introduces intrinsic splitting errors that are proportional to the time step used in the numerical solution (Fahs et al., 2009). These numerical artifacts can be avoided by using dense computational grids with small time steps, which increase the computational requirements and the CPU time of simulations. This limits the applicability of numerical models, especially in GCS applications that involve large time simulations for tens to hundreds of years at a large spatial scale. However, in the last years, advanced numerical methods (e.g., Mixed Hybrid finite elements (MHFE), Discontinuous Galerkin finite element (DGFE), Multipoints flux approximation approach (MPFA), error control based time stepping) have been developed for solving groundwater flow and transport equations in porous media. A detailed review of these numerical methods can be found in Miller et al. (2013) (Miller et al., 2013). These advanced numerical techniques allow for enhancing model applicability by improving the computational time while maintaining high accuracy. They have been applied to a wide range of problems involving groundwater flow, and transport processes (e.g., (Hirthe and Graf, 2012; Hoteit and Firoozabadi, 2018, 2008; Koohbor et al., 2020; Moortgat, 2017; Moortgat et al., 2016), but their applications to problems dealing with variable-density flow models are limited (Raeisi Isa-Abadi et al., 2020; Younes et al., 2009). To the best of our knowledge, none of these numerical methods have been yet applied to RTHC problems.

The objective of this paper is to address the above-discussed shortcomings of numerical simulations of reactive-convection of CO_2 in geological formations by i) developing a new robust numerical model based on advanced numerical techniques, and ii) investigating the effect of temperature on the processes of convective-reactive CO_2 dissolution. The numerical model is developed based on the combination of the MHFE method (Younes et al., 2010) for groundwater flow and the DGFE method (Miller et al., 2013; Raeisi Isa-Abadi et al., 2020) for mass and heat transfer. The combination of these methods has shown several advantages in generating accurate and efficient numerical solutions of the variable-density flow problems (Younes et al., 2009), but it has never been applied to RTHC processes. Flow, mass transport, heat transfer, and chemical dissolution are solved sequentially. An adaptive time-stepping procedure, based on error control, is implemented to avoid operator splitting errors. The advantages of this scheme in the time integration of variable-density flow problems is highlighted in (Hirthe and Graf, 2012; Younes and Ackerer, 2010). This approach is extended in this work to model reactive processes. The numerical model is compared to the commercial FE software COMSOL Multiphysics. The new model is used to understand the effect of temperature on the processes of convective-reactive CO_2 dissolution in a natural gas reservoir in the North-sea.

2. Conceptual model and method

2.1 The porous square benchmark: problem description

The numerical model developed in this work is adaptable for large-scale problems with complex geometries. However, as is common in the literature and theoretical research, we applied it to the problem of saturated porous square, which is widely accepted as a benchmark for several purposes such as understanding physical processes, comparing numerical codes, and evaluating the effect of aquifer characteristics on trapping process (Farajzadeh et al., 2011; A. Islam et al., 2014; Islam et al., 2013b; Kim et al., 2019). The popularity of this benchmark stems from the regularity of its geometry and the simplicity of the corresponding boundary conditions. Thus, our domain is a square of size $\mathrm{H}[\mathrm{m}]$, filled with saturated porous media. The domain is assumed to be homogenous. The boundary conditions for flow, mass, and heat transfer are demonstrated in Figure 1. Vertical walls are impermeable and adiabatic. The top wall of the domain is exposed to the constant concentration of solute $\mathrm{CO_2}$ $\left(C_{CO2}^{S}\left[M.L^{-3}\right]\right)$. No dispersive $\mathrm{CO_2}$ flux is imposed at the bottom surface. Hot $\left(\theta_H\left[\Theta\right]\right)$ and cold $\left(\theta_C\left[\Theta\right]\right)$ temperatures are applied to the bottom and top boundaries, respectively. These temperatures are representative of a geothermal temperature gradient. Initially, the fluid is at rest with no dissolved $\mathrm{CO_2}$ in the domain, and the fluid is at a reference temperature $(\theta_0\left[\Theta\right])$. Geochemical reactions occur between dissolved $\mathrm{CO_2}$ and calcium carbonate $\left(\mathrm{CaCO_3}\right)$. The relative non-dimensional concentration of $\mathrm{CaCO_3}$ is equal to $\mathrm{C}_{\mathrm{CaCO_3}}^{s}\left[M.L^{-3}\right]$ before the dissolution of $\mathrm{CO_2}$ in the water.

There are many models for CO_2 geological reactions. Levels of complexity and realism of these models depend on the intended application. The variability of models concerns the geochemical reactions as well as the laws used to describe the kinetic reactive processes. The simplified geochemical system considered in this work is widely used in the literature of convective CO_2 transport (e.g. Babaiee and Islam 2018, Tian and Wang 2017, Emami-Meybodi et al. 2015, Zhang et al. 2011). It assumes that dissolved CO_2 results in the formation of H_2CO_3(aq), HCO_3^- and CO_3^{2-}, as in the following reactions:

$$\begin{gathered} CO_2(aq)+H_2O\rightarrow H_2CO_3(aq) \\ H_2CO_3(aq)\leftrightarrow H^+(aq)+HCO_3^-(aq) \\ HCO_3^-(aq)\leftrightarrow H^+(aq)+CO_3^{2-}(aq) \end{gathered} \tag{1}$$

Dissolved CO2 reduces the pH, and in the zone of low-pH the concentration of cations (Ca^{2+}) increases, following these reactions:

$$CaCO_3(s)\leftrightarrow Ca^{2+}(aq)+CO_3^{2-}(aq) \tag{2}$$

2

The system can be reformulated using the Carbon dioxide (CO_2) and Calcium Carbonate $CaCO_3$ as primary species. As suggested by Babaiee and Islam (2018), Ghesmat et al. (2011) and Romanov et al. (2015), the chemical reactions can be summarized as follows:

$$CO_2\ (aq) + CaCO_3\ (s) \rightarrow Ca(HCO_3)_2\ (aq) \qquad (3)$$

The number of primary species is reduced to two by replacing the multicomponent geochemical system by equation (3). This assumes that the aquifer is entirely consisting of calcium carbonate and all the ions (Ca^{2+}, HCO_3^-, CO_3^{2-}) are replaced with calcium bicarbonate.

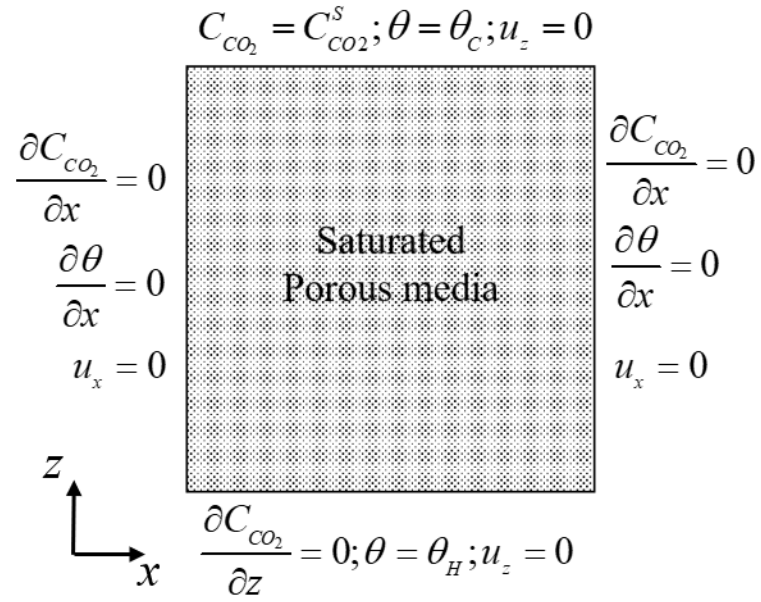

Figure. 1. Illustration of the conceptual model for GCS as a RTHC problem in a porous box.

2.2 The mathematical model

The governing equations describing the flow, mass and heat transfer and geochemical reactions processes are as follows:

- continuity equation with Boussinesq approximation:

$$\nabla . \boldsymbol{u} = 0 \qquad (4)$$

Where, $\boldsymbol{u}\left[L.T^{-1}\right]$ is the Darcy's velocity field.

- Darcy's law:

$$u_x = -\frac{k}{\mu}\frac{\partial p}{\partial x}; u_z = -\frac{k}{\mu}\left(\frac{\partial p}{\partial z} - \left(\rho - \rho_0\right) g\right) \tag{5}$$

Where, $u_x\left[L.T^{-1}\right]$ and $u_z\left[L.T^{-1}\right]$ are the horizontal and vertical components of Darcy's velocity field, respectively. $k\left[L^2\right]$ is the permeability of the porous media, $\mu\left[M.L^{-1}.T^{-1}\right]$ is the fluid viscosity, $p\left[M.L^{-1}.T^{-2}\right]$ is the fluid pressure, $\rho\left[M.L^{-3}\right]$ is the fluid density, and $g\left[L.T^{-2}\right]$ is the gravity acceleration.

- Mass conservation of the primary species (CO_2 and $CaCO_3$):

$$\phi\frac{\partial C_{CO_2}}{\partial t} + u_x\frac{\partial C_{CO_2}}{\partial x} + u_z\frac{\partial C_{CO_2}}{\partial z} = D.\phi\left(\frac{\partial^2 C_{CO_2}}{\partial x^2} + \frac{\partial^2 C_{CO_2}}{\partial z^2}\right) - K_r C_{CO_2}.C_{CaCO_3} \tag{6}$$

$$\phi\frac{\partial C_{CaCO_3}}{\partial t} = -K_r C_{CO_2}.C_{CaCO_3} \tag{7}$$

Where, $\phi[-]$ is the porosity, $C_{CO_2}\left[M.L^{-3}\right]$ is the concentration of CO_2, $C_{CaCO_3}\left[M.L^{-3}\right]$ is the mass fraction of $CaCO_3$ to the mass of rocks, $t[T]$ is the time, $D\left[L^2.T^{-1}\right]$ is the molecular diffusion coefficient, n is the reaction order, and $K_r[M^{-1}.L^3T^{-1}]$ is the reaction rate.

The reaction rate is modeled using the rate laws for kinetic reactions (Saaltink et al., 2001). In its rigorous form, when the full chemical system is considered, the reaction rate should be a function of the saturation index. However, as common for convective CO_2 transport, when the saturation index is very small and with the previous simplifications, the rigorous format can be substituted by a constant coefficient multiplied by the concentration of the primary species and mass fraction for the mineral.

- Energy balance:

$$\sigma \frac{\partial \theta}{\partial t} + u_x \frac{\partial \theta}{\partial x} + u_z \frac{\partial \theta}{\partial z} = \alpha \left(\frac{\partial^2 \theta}{\partial x^2} + \frac{\partial^2 \theta}{\partial z^2} \right) \tag{8}$$

- Where, $\sigma\left[-\right]$ is the ratio of heat capacity of the saturated porous domain to the fluid, $\theta\left[\Theta\right]$ is the temperature and $\alpha\left[L^2.T^{-1}\right]$ is the thermal diffusivity of the saturated porous domain.
- Temperature and concentration dependence on density (Tabrizinejadas et al., 2020):

$$\rho = \rho_0 (1 + \beta_C.C_{CO_2} + \beta_T (\theta - \theta_0)) \tag{9}$$

Where, $\rho_0\left[M.L^{-3}\right]$ is the density of native water at the reference temperature, $\beta_C[M^{-1}.L^3]$ and $\beta_T[\Theta^{-1}]$ are, respectively, the solute and thermal expansions, and $\theta_0[\Theta]$ is the reference water temperature.

- The temperature dependence of the reaction rate (Petrou, 2012):

$$K_r = A \exp\left(-\frac{E_a}{R.\theta} \right) \tag{10}$$

Where $A[M^{-1}.L^3 T^{-1}]$ is the pre-exponential factor, $E_a\left[M.L^2.T^{-2}\right]$ is the activation energy, $R\left[M.L^2.T^{-2}.\Theta^{-1}\right]$ is the ideal gas constant.

- The temperature dependence of the viscosity:

$$\mu(\theta) = C_0 + C_1 \times \theta + C_2 \times \theta^2 + C_3 \times \theta^3 + C_4 \times \theta^4 + C_5 \times \theta^5 + C_6 \times \theta^6 \tag{11}$$

The coefficients in equation (11) are given as follows: $C_0 = 1.37995$, $C_1 = -0.021224$, $C_2 = 1.360456 \times 10^{-4}$, $C_3 = -4.645409 \times 10^{-7}$, $C_4 = 8.9042735 \times 10^{-10}$, $C_5 = -9.0790692 \times 10^{-13}$ and $C_6 = 3.8457331 \times 10^{-16}$.

2.3 Dimensionless analysis

We perform our analysis based on the non-dimensional form of the governing equations. The following dimensionless variables are used:

$$X=\frac{x}{H};Z=\frac{z}{H};\boldsymbol{U}=\frac{\boldsymbol{u}.H}{\phi D};P=\frac{p.k}{\mu.\phi.D};\tau=\frac{t.D}{H^2};CO_2=\frac{C_{CO_2}}{C_{CO_2}^S};$$
$$CaCO_3=\frac{C_{CaCO_3}}{C_{CaCO_3}^S};\eta=\frac{\theta-\theta_C}{\theta_H-\theta_C} \tag{12}$$

By assuming that the reference temperature is $\theta_C\left(\theta_0=\theta_C\right)$ and $C_{CaCO_3}^S=C_{CO_2}^S$, the non-dimensional governing equations become as follow:

$$\nabla.\boldsymbol{U}=0 \tag{13}$$

$$U_X=-\frac{\partial P}{\partial X};U_Z=-\frac{\partial P}{\partial Z}+Ra_S.CO_2+Ra_T.Le.\eta \tag{14}$$

$$\frac{\partial CO_2}{\partial\tau}+U_X\frac{\partial CO_2}{\partial X}+U_Y\frac{\partial CO_2}{\partial Y}=\frac{\partial^2 CO_2}{\partial X^2}+\frac{\partial^2 CO_2}{\partial Z^2}-Da.CO_2.CaCO_3 \tag{15}$$

$$\frac{\partial CaCO_3}{\partial\tau}=-Da.CO_2.CaCO_3 \tag{16}$$

$$\sigma\frac{\partial\eta}{\partial\tau}+\phi.U_x\frac{\partial\eta}{\partial X}+\phi.U_z\frac{\partial\eta}{\partial Z}=\phi.Le\left(\frac{\partial^2\eta}{\partial X^2}+\frac{\partial^2\eta}{\partial Z^2}\right) \tag{17}$$

In equations (13) -(17), the dimensionless parameters are defined as follows:

- The local solute Rayleigh number expressing the ratio of solute buoyancy to solute diffusivity:

$$Ra_S=\frac{g.k.H.\rho_0.\beta_C.\Delta C_{CO_2}}{\phi.\mu.D} \tag{18}$$

where ΔC_{CO_2} is the difference between the highest and lowest concentration of C_{CO_2} in the domain. ΔC_{CO_2} is equal to $C_{CO_3}^S$ because the lowest C_{CO_2} concentration is assumed to be zero.

- The local thermal Rayleigh number, which is the ratio of thermal buoyancy to thermal diffusivity

$$Ra_T = \frac{g.k.H.\rho_0.\beta_T.\Delta\theta}{\mu.\alpha} \tag{19}$$

$\Delta\theta\left(=\theta_H - \theta_C\right)$ is the difference between the highest and lowest temperature.

- The Lewis number, expressing the ratio of thermal diffusivity to solute diffusivity, is

$$Le = \frac{\alpha}{\phi.D} \tag{20}$$

- The local Damköhler number giving the ratio of geochemical reaction rate to diffusion rate is given by

$$Da = \frac{K_r.C_{CO_2}^{s}.H^2}{\phi.D} \tag{21}$$

- The local Damköhler number is expressed as a function of temperature using the Arrhenius law):

$$Da = Da_0 \exp\left(-\frac{1}{R_1\eta + R_2}\right) \tag{22}$$

In equation (22), the parameters Da_0, R_1 and R_2 are defined as follows:

$$Da_0 = \frac{A.C_{CO_2}^{s}.H^2}{\phi.D} \tag{23}$$

$$R_1 = \frac{R\Delta\theta}{E_a} \tag{24}$$

$$R_2 = \frac{R\theta_c}{E_a} \tag{25}$$

2

2.4 A new numerical model for RTHC

A new numerical model is developed to solve the governing equations (equations (13)-(17)). The new model is based on advanced formulations of the FE method. Appropriate formulations are used to treat the different mathematical operators. The main goal behind selecting these advanced formulations is to reduce CPU time, while maintaining high accuracy. The new model is based on the in-house code TRACES (Transport of RadioACtive Elements in Subsurface) (Shao et al., 2018; Younes et al., 2009). TRACES is extended in this study to deal with RTHC simulations. In TRACES, the flow is discretized with the MHFE method, which is more accurate than the standard FE method in simulating fluid flow in heterogeneous porous domains (Younes et al., 2010). The advection operators in the mass transport and energy conservations are treated with the DGFE method (Miller et al., 2013; Raeisi Isa-Abadi et al., 2020). This method leads to high accuracy solutions as it reduces numerical diffusion and unphysical oscillations (Miller et al., 2013). The dispersion-diffusion operators for mass and heat transfer are discretized using the MPFA method (Younes et al., 2013) Advantages of this combination of FE formulations have been discussed in (Fahs et al., 2016; Shao et al., 2018; Tabrizinejadas et al., 2020). The equations of flow, mass transfer and energy balance, under variable density, are solved sequentially. The reactive operator is also coupled to the flow and transfer processes with the sequential non-iterative approach. However, it is known that this approach introduces operator splitting errors proportional to the time step (Fahs et al., 2008). To control this error, we implement an adaptive time-stepping based on error estimation. The time step is adapted during the simulation based on error control to maintain the prescribed accuracy. Thus, after each time level, the next time step is calculated automatically in a way that error is less than the prescribed accuracy. The error is evaluated using the traction order of the Taylor series. More details about this time integration scheme can be found in Hirthe and Graf (2012) and Younes et al. (2010).

3. Comparaison TRACES vs. standard FE solutions

3.1 Verification

A new code (TRACES) has been developed to simulate RTHC of $\mathrm{CO_2}$. This section aims at verifying the correctness of the new developed code. Thus, TRACES is compared to a FE solution obtained using COMSOL Multiphysics. The COMSOL model is developed by coupling the modules of 'Darcy's Law –*dl*', 'Heat Transfer in Porous Media –*ht*' and 'Transport of Diluted Species in Porous media –*tds*'. The reaction term is defined as a function of temperature and it is included in '*tds*' module as in equation (10). This equation is implemented in COMSOL as 'variables' in "component definition". The density is assumed to be a function of temperature and concentration as in equation (9). The Boussinesq approximation is implemented in COMSOL by assuming constant density in the three modules ('*dl*', '*ht*' and '*tds*') and including variable density in the gravity term. The viscosity is considered as a function of temperature as in equation (11).

In our analysis, we use quantitative metrics, which can be helpful for validating and benchmarking numerical codes. As common in the literature, we use the average Nusselt ($\overline{Nu}$) and Sherwood ($\overline{Sh}$) numbers to characterize the rates of heat and mass transfer to the domain, respectively. $\overline{Nu}$ and $\overline{Sh}$ are defined as follows (Rajabi et al., 2020):

$$\overline{Nu} = \int_0^1 \left.\frac{\partial \eta}{\partial Z}\right|_{Z=0} dX \qquad (2)$$

$$\overline{Sh} = \int_0^1 \left.\frac{\partial CO_2}{\partial Z}\right|_{Z=1} dX \qquad (27)$$

For evaluating the capacity of the reservoir in capturing $\mathrm{CO_2}$, we use the total diffusive flux at the domain top surface (TF^{diff}). This is defined as a time integral of the instantaneous flux. At a dimensionless time $\tau *$, TF^{diff} is calculated as follows:

$$TF^{diff} = \int_0^{\tau^*} \overline{Sh}\, d\tau \tag{28}$$

Verification in the case of vertical concentration and temperature gradients is questionable due to the gravitational instability. Therefore, we considered a stable configuration by considering horizontal temperature and concentration gradients. Thus, Dirichlet boundary conditions of temperature and concentration on the vertical walls of the domain and assuming that there is no heat and mass fluxes across the horizontal walls. This case is inspired from (Tabrizinejadas et al., 2020).In order to avoid potential numerical oscillations in the FE solution, the comparison between TRACES and COMSOL is made for a test case with a smooth distribution of concentration and temperature (low convective flow regime and relatively slow reaction rate). This case is denoted by 'Test case 1-H', referring to horizontal concentration and temperature gradient. The non-dimensional parameters for this test case are listed in Table 1**Erreur ! Source du renvoi introuvable.**. The corresponding physical parameters used in COMSOL are given in Table 2. Parameters in these tables are physically plausible and consistent (Sainz-Garcia et al., 2017). The viscosity is assumed to be independent of temperature (i.e. $\mu = \mu_0$) to ensure constant thermal and solution Rayleigh numbers. To alleviate nonlinearity, we assume a first-order dissolution reaction. Thus, in equation (6), the reaction term ($-K_r C_{CO_2} . C_{CaCO_3}$) is replaced by $-K_r C_{CO_2}$. In other words, the concentration $CaCO_3$ is assumed to be constant (i.e. equal to $\mathrm{C}^s_{\mathrm{CaCO_3}}$) in the reaction term. This term is dropped from the equations when C_{CaCO_3} becomes null.

A triangular mesh of about 12K nodes is used in the simulations, for both COMSOL and TRACES. This mesh has been generated using the meshing tool in COMSOL. The flow, mass transport and heat transfer equations in COMSOL are solved simultaneously via the fully implicit approach. The time stepping technique is based on the Backward differentiation formula. The order of the formula as well as the size of the time steps are updated automatically in order to reach the prescribed accuracy. The relative accuracy is set to 10^{-6}. Same relative accuracy is considered for the time stepping in TRACES. The comparisons between the results of 'Test case 1-H' obtained from TRACES and COMSOL are demonstrated in Figure 2. The dimensionless concentration and temperature distributions are plotted at a non-dimensional time $\tau = 0.05$, and the metrics characterizing mass and heat transport are plotted over time. Both solutions are indistinguishable in terms of concentration (CO_2 and $CaCO_3$) and temperature distributions as well as for $\overline{Nu}$, $\overline{Sh}$ and TF^{diff} . For the case of horizontal temperature and concentration gradients, these metrics are defined at the left vertical wall. These results confirm not only the correctness of the developed TRACES code, but also the COMSOL model and the post-treatment analysis for the evaluation of metrics used for characterizing the mass and heat transfer processes.

Table 1. Non-dimensional parameters used for the test cases

	'Test case 1-V' and 'Test case 1-H'	'Test case 2'	'Test case 3'
Ra_S	300	800	1000
Ra_T	30	80	1000
Le	2	5	10
Da_0	10^{11}	5×10^{11}	10^{11}
R_1	10^{-3}	10^{-2}	10^{-2}
R_2	5×10^{-2}	7×10^{-2}	5×10^{-2}
ϕ	0.3	0.3	0.3
σ	0.46	0.46	0.46

2

Table 2. Dimensional parameters used for the test cases

Gas constant	$R = 8.314 J.mol^{-1}.K^{-1}$
Reference Temperature	$\theta_0 = 277.15K$
Porous box size	$H = 1m$
Porosity	0.3
Concentration of CO_2 at the inlet wall	$C^S_{CO_2} = 1$ mol.m^{-3}
Initial concentration of $CaCO_3$	$C^s_{CaCO_3} = 1$ mol.m^{-3}
Freshwater density	$\rho_0 = 1000$ kg.m^{-3}
Solid phase density	$\rho_s = 2300$ kg.m^{-3}
Gravity	$g = 10$ m.s^{-2}
Viscosity	$\mu_0 = 10^{-3}$ kg.m^{-1}.s^{-1}
Permeability	$k = 10^{-9}$ m^2
Cold temperature	$\theta_C = 277.15$ K
Thermal capacity of water	$cp_f = 4200$ J.kg^{-1}.K^{-1}
Thermal capacity of soil	$cp_s = 418$ J.kg^{-1}.K^{-1}
Thermal Conductivity of water	$\lambda_f = 0.65$ W.m^{-1}.K^{-1}
Thermal Conductivity of soil	$\lambda_s = 5.725$ W.m^{-1}.K^{-1}

	'test case 1-H and V'	'test case 2'	'test case 3'
Thermal expansion coefficient of water	$\beta_T = 5.5\times10^{-4}$K^{-1}	$\beta_T = 2.05\times10^{-4}$K^{-1}	$\beta_T = 0.001$K^{-1}
Hot temperature	$\theta_H = 282.61^\circ$K	$\theta_H = 316.17^\circ$K	$\theta_H = 332.58^\circ$K
Mass Expansion	$\beta_C = 0.015$ m^3.mol^{-1}	$\beta_C = 0.016$ m^3.mol^{-1}	$\beta_C = 0.01$m^3.mol^{-1}
Molecular Diffusion	$D_m = 1.67\times10^{-6}$ m^2.s^{-1}	$D_m = 6.67\times10^{-7}$ m^2.s^{-1}	$D_m = 3.33\times10^{-7}$ m^2.s^{-1}
Activation Energy	$Ea = 45419$ J.mol^{-1}	$Ea = 32442$ J.mol^{-1}	$Ea = 46085$ J.mol^{-1}
Pre-exponential factor in the Arrhenius law	$A = 5\times10^4$ s^{-1}.m^{-3}.mol	$A = 5\times10^4$ s^{-1}.m^{-3}.mol	$A = 10^4$ s^{-1}.m^{-3}.mol

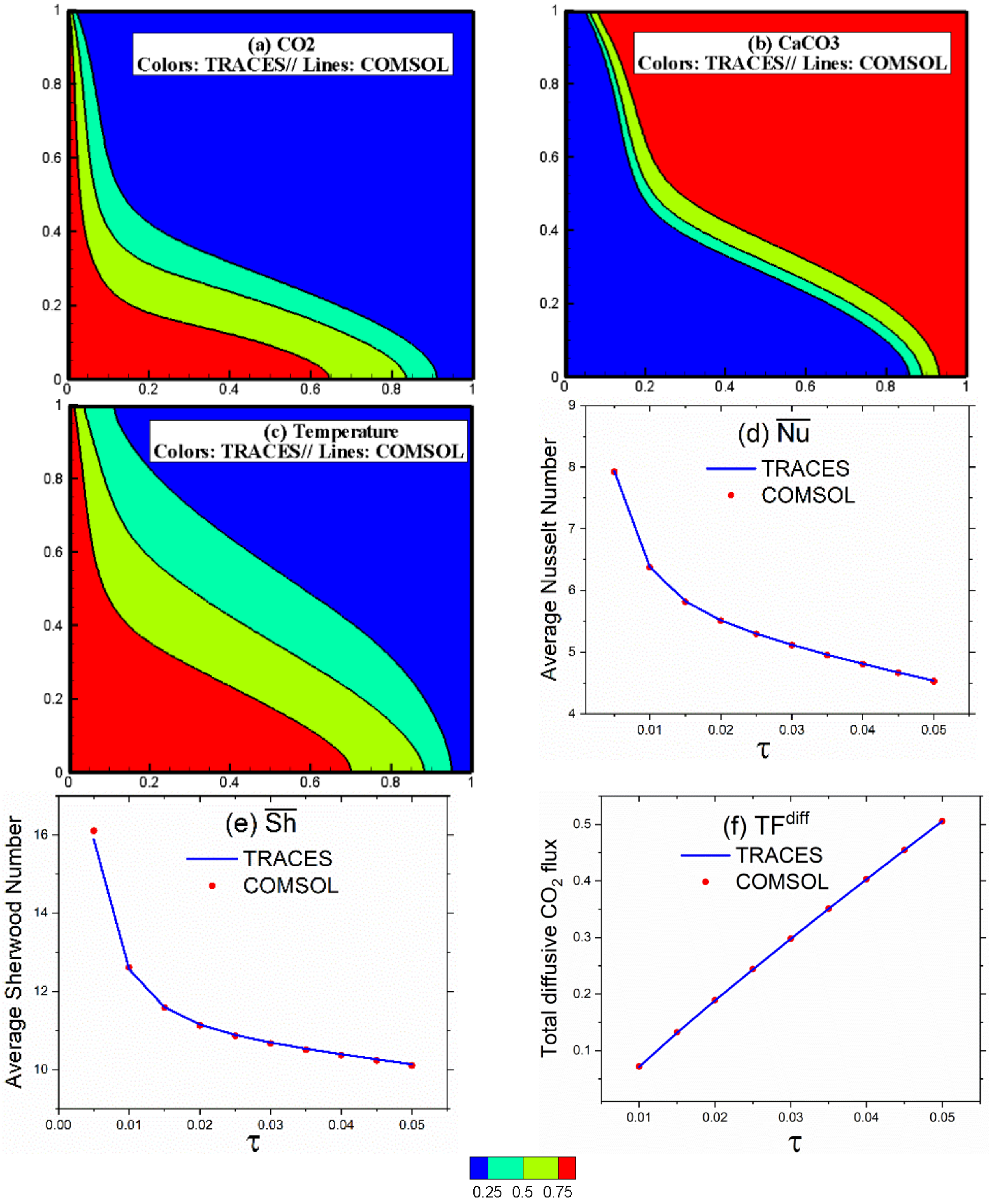

Figure. 2. 'Test case 1-H': Comparison between TRACES and COMSOL for (a) dimensionless CO_2 concentrations, (b) dimensionless $CaCO_3$ concentration, (c) dimensionless temperature distribution at $\tau = 0.05$, (d) $\overline{Nu}$, (e) $\overline{Sh}$ and (f) TF^{diff}.

We also compared the results of TRACES versus COMSOL in the case of vertical temperature and concentration gradients, involving gravitational instability. This test case is called 'Test case 1-V', referring to vertical concentration and temperature gradients (see Figure 1). The non-dimensional parameters are kept the same as 'Test case 1-H'. The same computational mesh and time step, as in 'Test case 1-H', is used in the analysis of 'Test case 1-V'. Thus, numerical artifacts related to space or time discretization can be avoided. The comparison between the results of TRACES and COMSOL for dimensionless concentrations (CO_2 and $CaCO_3$) and temperature (at $\tau = 0.05$) as well as $\overline{Nu}$, $\overline{Sh}$ and TF^{diff} (over the time) are shown in Figure 3. This figure shows that both models provide equivalent results. Despite the equivalent numerical parameters used for time integration and spatial discretization, both models are not in full agreement. However, this agreement can be seen as satisfactory, knowing that, in the literature, matching results of this unstable configuration in space and time is somewhat unsuccessful (Xie et al., 2012). An important observation is that good agreement between COMSOL and TRACES is obtained for the total flux, which is the most important model output for the evaluation of reservoir capacity in capturing CO_2. This means that numerical instability does not materially affect the total flux of CO_2.

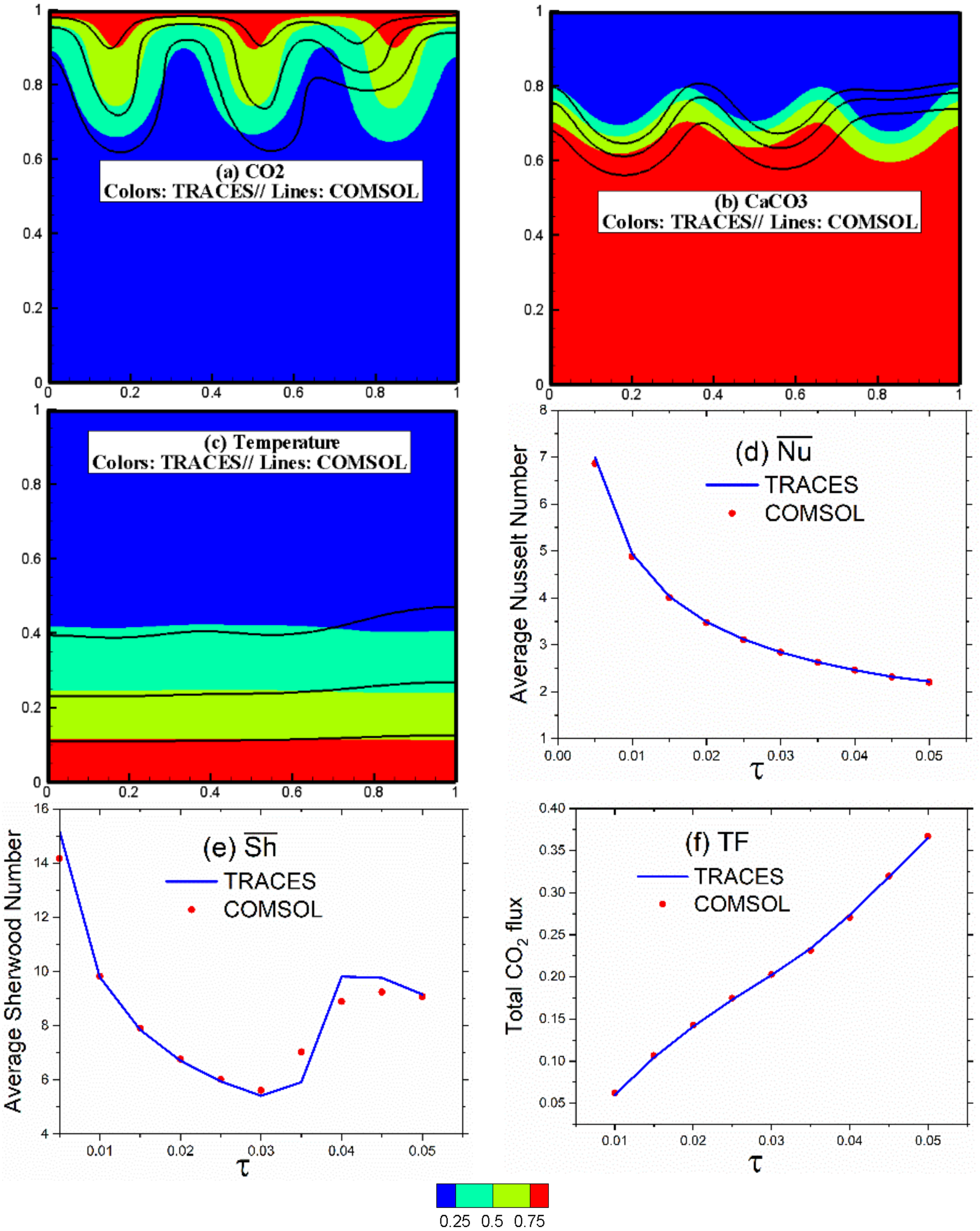

Figure 3. Comparison between TRACES and COMSOL for 'Test case 1'V': (a) dimensionless CO_2 concentrations, (b) dimensionless $CaCO_3$ concentration, (c) dimensionless temperature, all at $\tau = 0.05$. (d) time variation of $\overline{Nu}$, (e) time variation of $\overline{Sh}$ and (f) time variation of TF

3.2 Advantages of the newly developed model (TRACES)

One of the objectives of this work is to develop an accurate model for the simulation of RTHC processes, based on advanced FE methods and time integration techniques. This section aims at investigating the advantages of this newly developed model (TRACES), compared to the standard FE method (COMSOL). Several numerical schemes are available with COMSOL. In this work, we use the numerical scheme suggested by default in COMSOL, which is based on first order finite element scheme for the discretization of the mass transport equation and quadratic order finite element scheme for the discretization of the flow equation. This scheme is supposed to be the most suitable for the selected physics. It is selected in this work to imitate standard numerical schemes commonly implemented in commercial codes. We consider a challenging case dealing with sharp temperature and concentration distributions, and high Damköhler number. This test case is challenging because sharp temperature and concentration distributions may lead to unphysical oscillations or introduce numerical diffusion, while fast reaction rate requires small time steps to avoid operator splitting errors. This test case is denoted as ‘Test case 2’. As a mesh independent solution is required to compare the models, we limited this part to the case of horizontal thermal and solute gradients. This reference solution cannot be easily obtained in the case of vertical concentration and temperature gradients because inherent instability renders the solutions highly sensitive to the mesh. The non-dimensional parameters for ‘Test case 2’ are listed in Table 1. The physical parameters used in COMSOL are given in Table 2. As for ‘Test case 1’ the viscosity is assumed to be independent on temperature (i.e. $\mu = \mu_0$) and first-order dissolution reaction is considered.

A mesh-independent solution is obtained using TRACES with a mesh consisting of 12K nodes. With the same mesh, the FE solution (i.e., concentrations and temperature distributions) is different (Figures 4a-4c). The resulting FE solution exhibits spurious/unphysical oscillations. Examples of these oscillations are plotted in Figure 5. With the mesh consisting of 12K nodes, low negative concentrations are obtained for CO_2 (maximum negative value is -0.0066) (Figure. 5a). Due to the nonlinearity of the reaction term, these small oscillations in CO_2 lead to incoherent results of CaCO3 with, for instance, negative concentrations (until -1.72) and larger values beyond physics (+1.93) (Figures. 5b and 5c). The difference between TRACES and FE solutions can be attributed to the unphysical oscillations encountered with the FE method. These solutions are reduced (even avoided) with the numerical scheme used in TRACES.

By refining the mesh progressively, we observed that the FE solution is mesh-dependent. The simulation with 140K nodes is represented in Figures 4a-4c. The results are plotted for non-dimensional time $\tau = 0.05$. It is clear that, by refining the mesh, FE solution is converging towards the TRACES solution. But there is no full agreement between both solutions. A finer mesh should be used to get the same solution obtained with TRACES. But we stopped the mesh refinement at 140K nodes due to CPU time limitations. The oscillations are smoothed out with mesh refining, as can be seen in Figure 5. For CO_2, very small negative values are observed (the maximum negative value is -6×10^{-6}) (Figure 5d). Oscillations of $CaCO_3$ have been effectively reduced with mesh refining, but they remain significant (Figures 5e and 5f). The maximum negative concentration is -0.33, and the largest value beyond 1 is 1.096. These results indicate the agreement between TRACES and the FE solution is improved when the oscillations in the FE method are reduced by mesh refinement. This confirms that the discrepancy between both solutions is related to the oscillations encountered with the FE method. The results of this test case show that simulating RTHC processes at high Rayleigh and Damköhler numbers is challenging for the standard finite element method. This test case can be used as a benchmark for comparing newly developed methods in future studies. For the nodes of 12K nodes, the FE method is slightly more efficient in CPU time than TRACES. CPU time with the FE method is about 3000s while with TRACES it is about 5000s. This is because the DG method in TRACES have more degree of freedom. However, CPU time should be compared at equivalent accuracy.

This means that, in our case, the TRACES solution obtained with 12K nodes should be compared to the FE solution obtained with 140K nodes. The CPU time for this later is about 50 000s (about 14h). Thus, TRACES is 10 times more efficient than FE solution.

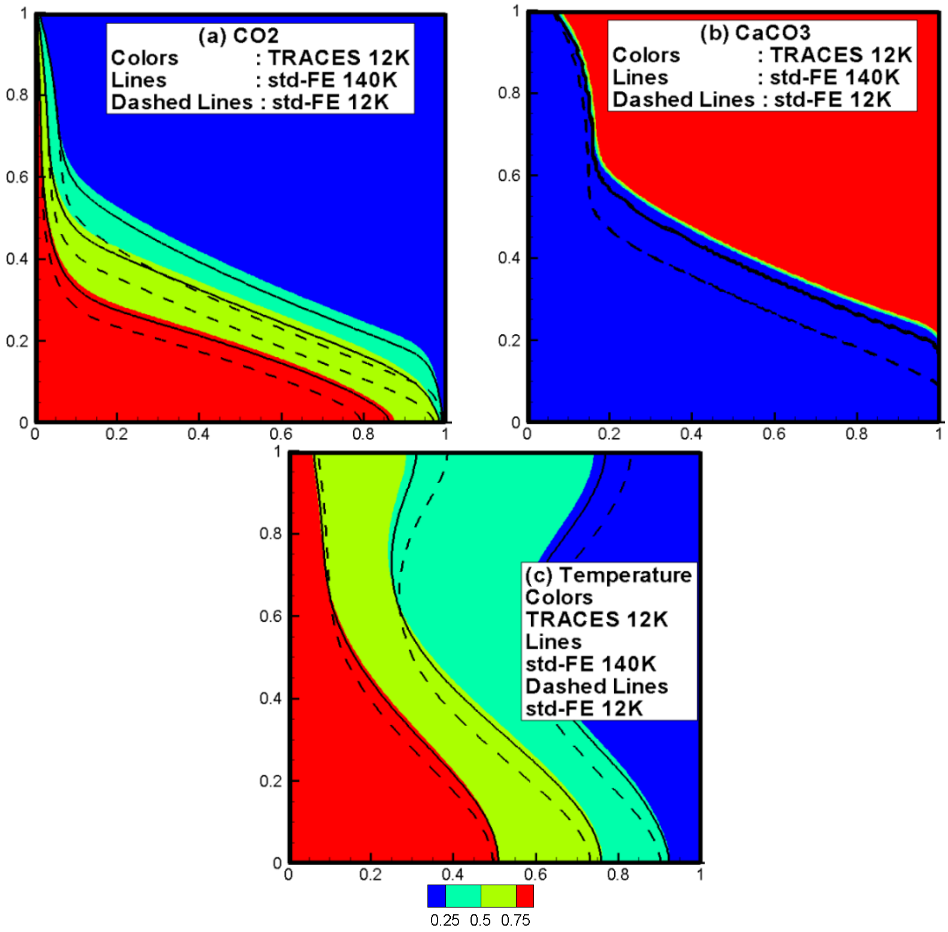

Figure 4. Comparison between TRACES and std-FE for ‘Test case 2’: (a) dimensionless CO_2 concentration, (b) dimensionless $CaCO_3$ concentration, (c) dimensionless temperature, all at $\tau = 0.05$.

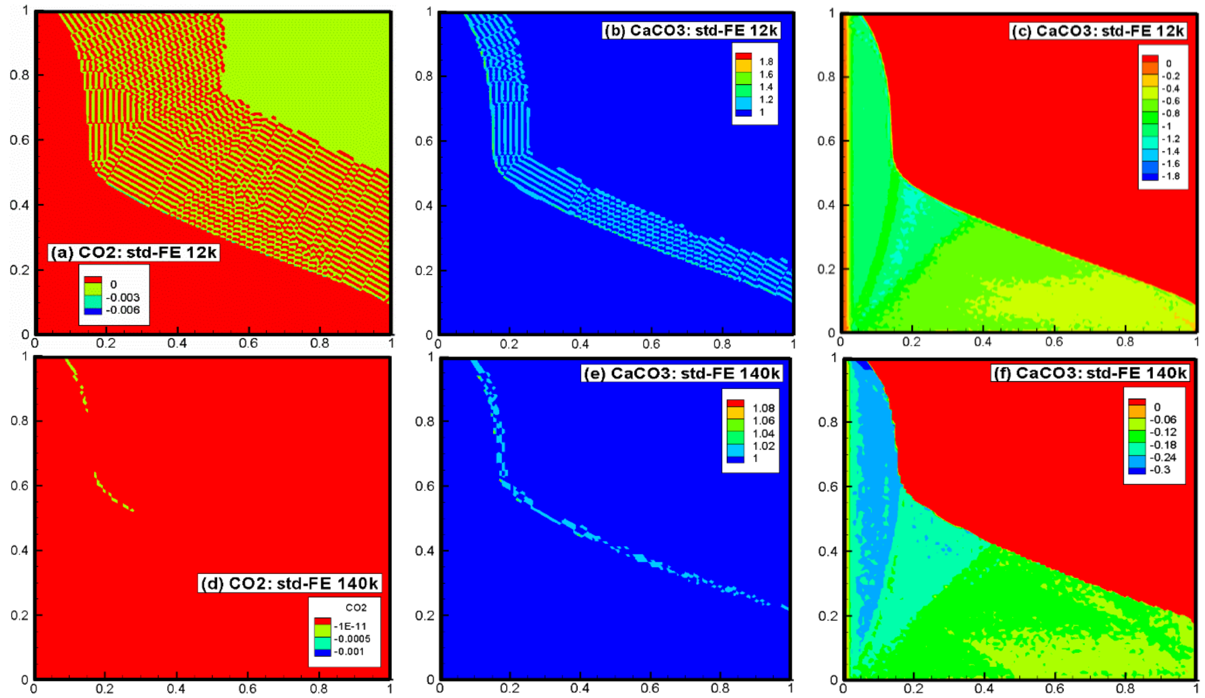

Figure 5. Oscillations with the std-FE solution for 'Test case 2'. Negative CO_2 concentration (a and d), $CaCO_3$ concentrations larger than one and (b and e) and negative $CaCO_3$ concentration (c and f). All the results are presented at $\tau = 0.05$.

4. Effect of temperature on the processes of convective-reactive CO_2 dissolution

Temperature gradient causes convective flow associated with density and viscosity dependence on temperature. It can also affect the reaction rate of the geochemical dissolution reactions. This section aims at investigating the effects of temperature on the process of convective-reactive CO_2 dissolution. For the first timeF, this is done based on the porous square benchmark described in section 2.1. This allows for understanding the thermal effect under simplified conditions (i.e., small scale and homogenous domain). Then a field case study in an offshore reservoir at the North Sea is investigated for a wider understanding under more realistic conditions such as heterogeneity and large space and time scales.

Our analysis is based on the comparison of three models with increasing levels of complexity and realism. The different simplifications and assumptions of these models are discussed below:

- Model 1 ('Isothermal'): In this model, the isothermal conditions are considered by assuming that the temperature is constant, in space and time. In this model, the density is assumed to be a function of concentration while the reaction rates and the viscosity are constant. The latter is calculated as a function of the constant temperature via equations (10) and (11), respectively. This model is called ‘isothermal’. It imitates models usually used in previous studies, which are based on isothermal assumptions.

- Model 2 (‘Linear Temperature’): This model assumes linear distribution of temperature with depth. The temperature is increasing with depth, but it is invariant in time. The viscosity and density are assumed to be independent of temperature, thus thermal convective processes are neglected. But, the reaction rate is assumed to be a function of temperature as in equation (10). This model is referred as ‘Linear Temperature’ in the rest of this paper.
- Model 3 (‘RTHC’): in this model, all the RTHC processes are included. Thus, the temperature is assumed to be a function of time and space. It is obtained by solving the heat transfer equation (Equation (8)). Density, viscosity, and reaction rate are assumed to be a function of temperature. This model is called ‘RTHC’.

The three models are used to simulate both the porous square cavity problem and the field case study. Several metrics such as the temperature and concentration distributions, the cumulative total flux of CO_2 at the top surface, and the total amount of $CaCO_3$ are used in the analysis. The comparison between models “Isothermal” and “Linear temperature” allows for investigating the effect of the temperature dependence of the reaction rate on these metrics. Comparison between models “Linear Temperature” and “RTHC” allows for understanding the effect of convective flow on the dissolution processes.

4.1 The hypothetical benchmark of porous square cavity

The dimensionless analysis of this benchmark (see section 2.3) shows that the processes of RTHC are governed by six non-dimensional parameters: Ra_S, Ra_T, Le, Da_0, R_1 and R_2. This paper does not address the impact of these parameters on CO_2 metrics. It aims at addressing the effect of neglecting heat processes on convective-reactive CO_2 processes. This is why we focus on the models dealing with different assumptions of thermal processes with two ranges of Rayleigh numbers. We first run the three models (“Isothermal”, “Linear Temperature” and “RTHC”) with the parameters used for ‘Test case 1’ dealing with low thermal Rayleigh number (see Tables 1 and 2). For “Isothermal”, Ra_T and Le are set to be 0. The local Damköhler number is calculated as in equation (22) with a constant dimensionless temperature $\eta = 0.5$. For the model “Linear Temperature” Ra_T and Le are also set to be 0, but the local Damköhler number is calculated as in equation (22) with a dimensionless temperature that varies linearly between 0 and 1 along the depth. For ‘Test case 1’, the simulations show equivalent results between the three models. These results are not presented for the sake of brevity. This indicates that at low Rayleigh numbers, at a small scale, and under homogenous configuration, the temperature has no effect on CO_2 concentration nor the metrics characterizing CO_2 storage and flux. We further investigate this benchmark at a higher thermal Rayleigh numbers. Thus, we consider a new test case (‘Test case 3’) dealing with a higher Rayleigh numbers and higher dependency of the reaction rate to temperature. Second-order dissolution reaction is assumed in this test case, as in equations (15) and (18). The non-dimensional parameters of this test case are given in Table 1 (‘Test case 3’). Ra_T and Le in this table are used only in “RTHC” model. For “Isothermal” and “Linear Temperature”, these parameters are set to zero. The physical parameters of ‘Test case 3’ are given in Table 2. The dependency of the Damköhler number to the temperature is plotted in Figure 6. This figure shows high variability of the Damköhler number with temperature with values ranging from 200 to about 6,000. These values are coherent with the range of variability of the Damköhler number considered in (Sainz-Garcia et al., 2017).

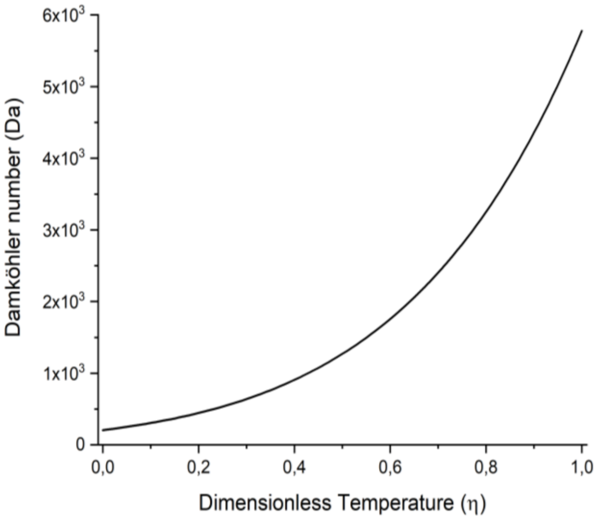

Figure 6. Variation of the Damköhler number as a function of dimensionless temperature in 'test case 3'.

Figure 7 shows the contour maps of normalized concentration of CO_2, $CaCO_3$, and temperature at $\tau = 0.01$ (equivalent to $30000s$) for 'Test case 3', simulated with three models. Density-driven fingering processes are observed with the three models. Equivalent results have been obtained with "Isothermal" and "Linear Temperature". However, the growth and depth development of fingers seem to be under-predicted with 'Isothermal" (Figures 7a and 7d). This can be related to the fact that, near the domain top surface, the temperature with "Isothermal" is higher than that with "Linear temperature" (see Figures 7c and 7f). Thus, in this zone, the local reaction rate is higher with "Isothermal" than with "Linear temperature". Faster dissolution of CO_2 leads to less penetration of fingers in the domain. To confirm this conclusion, we further simulate 'Test case 3' with "Isothermal" by assuming lower constant temperature ($\eta = 0.25$). The results (not shown for the sake of brevity) indicate more penetrated fingers with a reduced constant temperature. Figures 7b and 7e show a wider layer of $CaCO_3$ dissolution with "Linear temperature". This is coherent with the results of CO_2 showing rapid fingers penetration with this model. However, at the top surface of the domain, lower concentration of $CaCO_3$ can be observed with "Isothermal", indicating more local dissolution with this model. This is related to the fact that "Isothermal" over-predicts the reaction rate in this zone. With

$_2$

RTHC, unlike “Isothermal” and “Linear temperature”, due to opposite thermal (upward) and solute (downward) gradients, the convective CO_2 fingers are irregular and not uniformly distributed. Temperature distribution is also affected by both thermal and solute buoyancy effects (Figure 7i). Due to thermal convective processes (Figure 7i), CO_2 reaches the bottom surface of the domain but with low concentration (Figure 7g). Dissolution of CaCO3 takes place almost overall the domain. In the bottom surface, despite low concentrations of CO_2, significant dissolution processes can be observed (Figure 7h). The $CaCO_3$ concentration in this zone is almost zero. The high temperature at the bottom surface leads to a high reaction rate and enhances the dissolution processes.

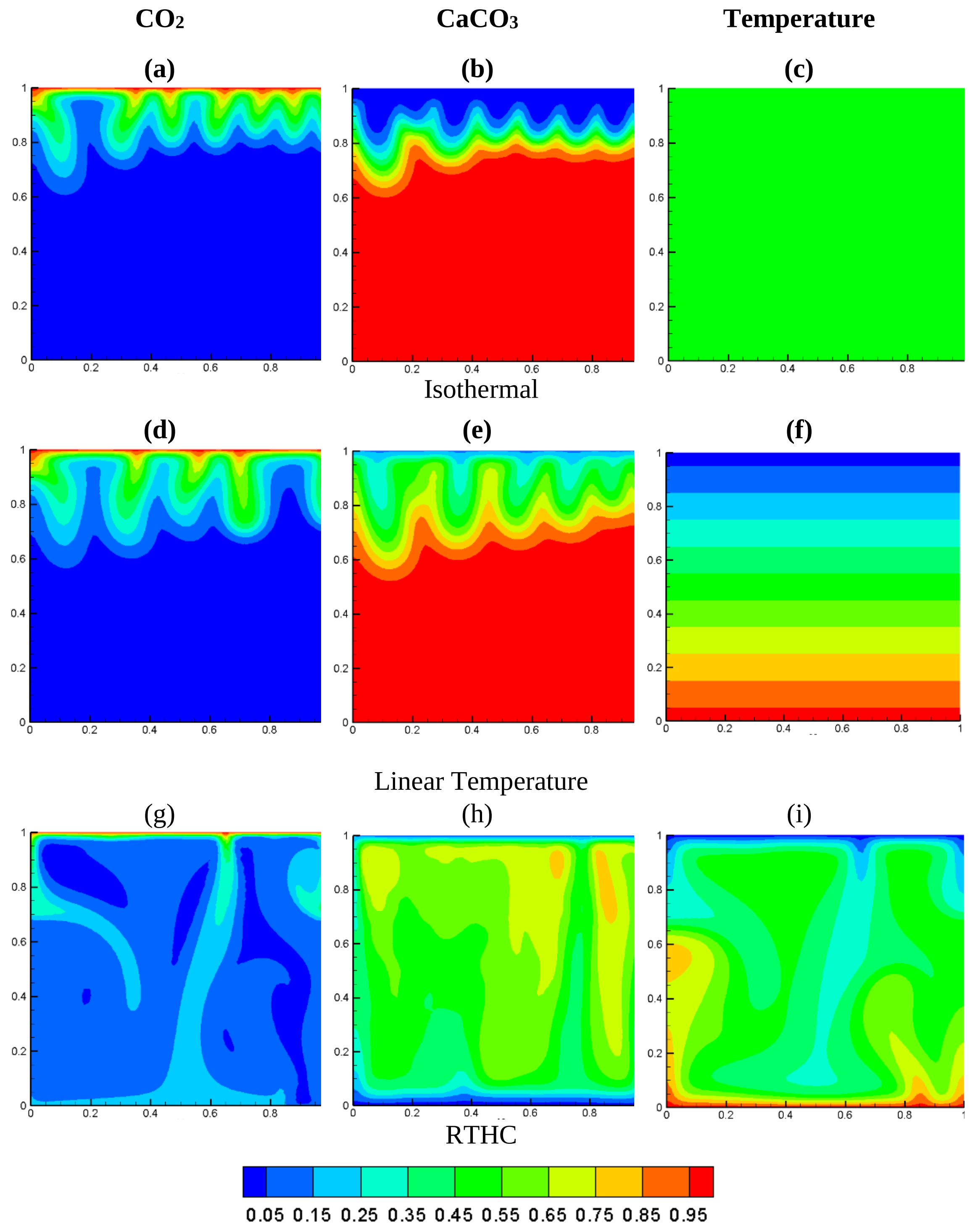

Figure 7. Dimensionless concentration of CO_2 (left) and $CaCO_3$ (middle) and dimensionless temperature (right) for 'test case 3' with the three models at $\tau = 0.01$.

In the previous sections, Nusselt and Sherwood number are used to discuss the accuracy of the newly developed numerical model. As common in the literature (Tabrizinejadas et al., 2020), these numbers are used to provide quantitative comparison between different models. In this section, as the main goal is understanding the effect of temperature on convective processes of CO_2 we used more relevant outputs, as follows:

- The non-dimensional metric giving the total amount of $CaCO_3$ available in the domain is given by:

$$T_{CaCO_3} = \int_0^1 \int_0^1 CaCO_3 dXdZ \tag{29}$$

- The instantaneous total flux of CO_2 at the top surface:

$$TF_{CO_2} = \int_0^1 \left(U_z CO_2 - \frac{\partial CO_2}{\partial Z} \right) dX \tag{30}$$

- The cumulative total flux of CO_2 at the dimensionless time τ:

$$TF_{CO_2}^{Cum} = \int_0^{\tau} TF_{CO_2} d\tau \tag{31}$$

These metrics are investigated for a non-dimensional duration ($\tau_{\max}$) of 0.01, which is equivalent to $30000s$. Figure 8a plots the variation of the total amount of $CaCO_3$ available in the domain with time, with the three models. Due to the dissolution processes, the three models show that the total amount of $CaCO_3$ is decreasing with time. “Linear temperature” leads to larger T_{CaCO_3} than “Isothermal”, during all the simulated periods. This is coherent with the results of the previous section showing fast dissolution of $CaCO_3$ with “Isothermal”. During the first period of simulation ($\tau < 0.0025$), both models “Linear temperature” and “RTHC” give similar results. This is related to the fact that, at this stage, the convection flow is still not affecting the temperature distribution. Thus, this distribution is linear, and in consequence “Linear Temperature” and “RTHC” are equivalent. For $\tau > 0.0025$, with “RTHC” the initial linear temperature distribution is disturbed by the convective flow. Due to convection processes, high temperatures can be found in the domain, which can be associated to higher reaction rates. In consequence, fast dissolution processes occur. This explains the faster decrease of T_{CaCO_3} with “RTHC” than “Linear Temperature”.

Figure 8b illustrates the time variation of the instantaneous total flux of CO_2 at the domain top surface (TF_{CO_2}). Similar behaviors can be observed with the three models, with a period of decreasing variation at the beginning of the simulation, followed by a period of increasing variation until becoming almost constant. This figure shows equivalent results between models “Isothermal” and “Linear temperature”. During a short time at the beginning of the simulation, the convective processes are absent. The CO_2 flux is induced by the mass diffusion between the zones of high concentration at the top surface and low concentration within the domain. When CO_2 infiltrates into the domain by diffusion, the concentration gradient at the top surface decreases, and in consequence, the CO_2 flux decreases. After this short period of purely diffusion transport, convective flow starts due to solute buoyancy effects in “Isothermal” and “Linear temperature” models and both thermal and solute buoyancy effects in “RTHC”. Convective processes enhance the CO_2 flux at the domain top surface. This explains this regime of increased CO_2 flux after the first period of decreased variation. Once the convective flow is well-established, the CO_2 flux becomes stable, as it can be seen in Figure 8b. From this figure, it is clear that “RTHC” leads to higher CO_2 flux than “Isothermal” and “Linear temperature”. These latter two models under-predict the CO_2 flux because they do not take into account the thermal convective processes.

The time variations of cumulative CO_2 flux obtained with the three models are given in Figure 8c. Equivalent results can be observed with “Isothermal” and “Linear temperature” models. These models, by considering simplified assumptions of the temperature field, under-predict the total CO_2 flux. The discrepancy between the results of “RTHC” and other models is increasing with time.

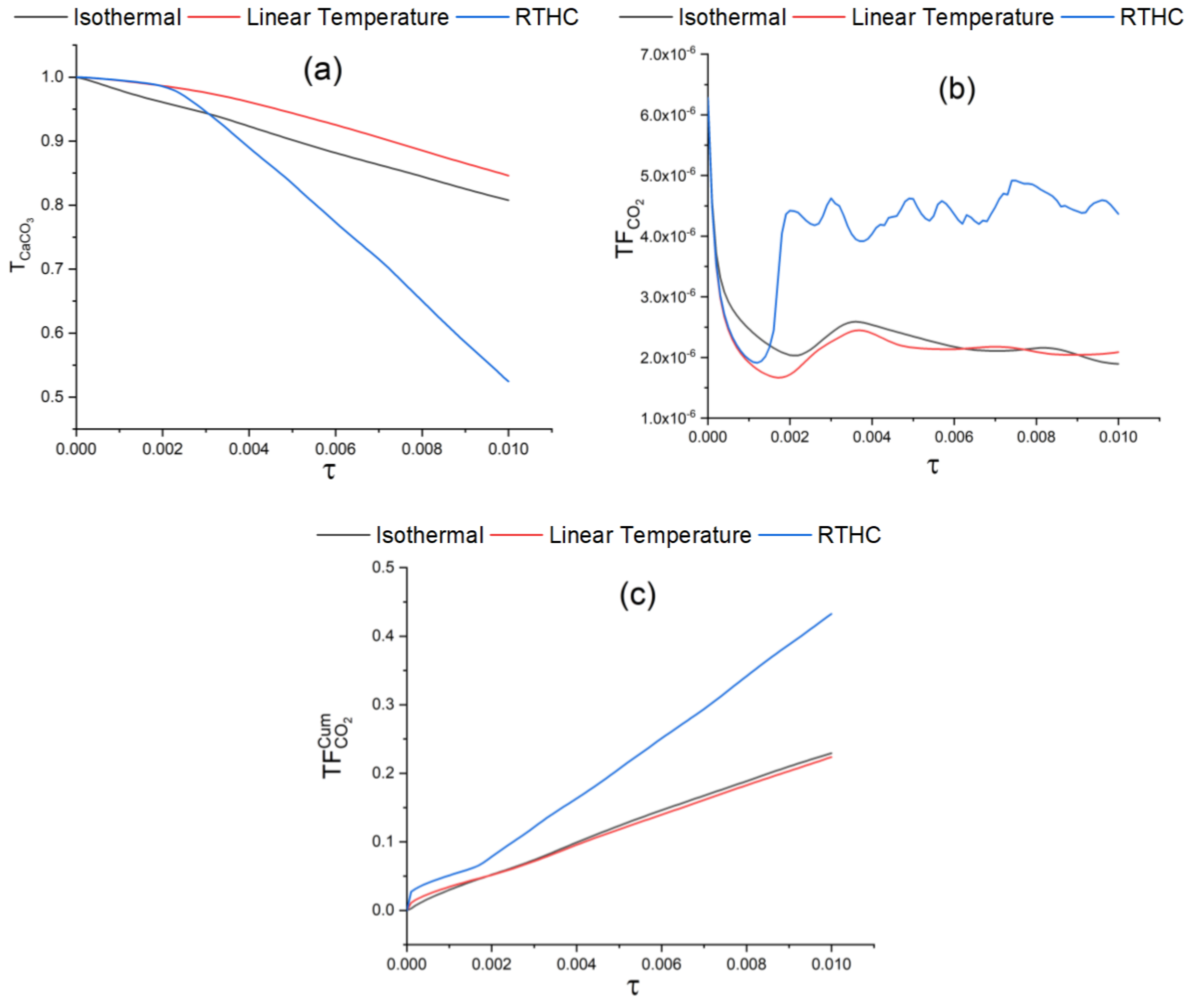

Figure 8. Time variations of the metrics characterizing $CaCO_3$ and CO_2 with the three models "Isothermal", "Linear temperature" and "RTHC": (a) the total amount of $CaCO_3$ available in the domain (T_{CaCO_3}), (b) the instantaneous total flux of CO_2 at the top surface (TF_{CO_2}) and (c) The cumulative total flux of CO_2 ($TF_{CO_2}^{Cum}$).

4.2 Field study: The Viking field in the North Sea

Previous studies on the effect of temperature on the processes of convective-reactive CO_2 dissolution are limited to hypothetical problems (A. Islam et al., 2014; A. W. Islam et al., 2014; Islam et al., 2013c). To the best of our knowledge, this topic has never been investigated for a real field application. The effect of heat on convective flow and geochemical reaction of CO_2 at large scale and under real geologic configuration is still not well understood. To address this gap, we investigate RTHC processes of CO_2 in a natural gas reservoir at the Viking field in the

North Sea in England, which is under consideration for CO_2 storage (Hoteit et al., 2019; Omar et al., 2021).

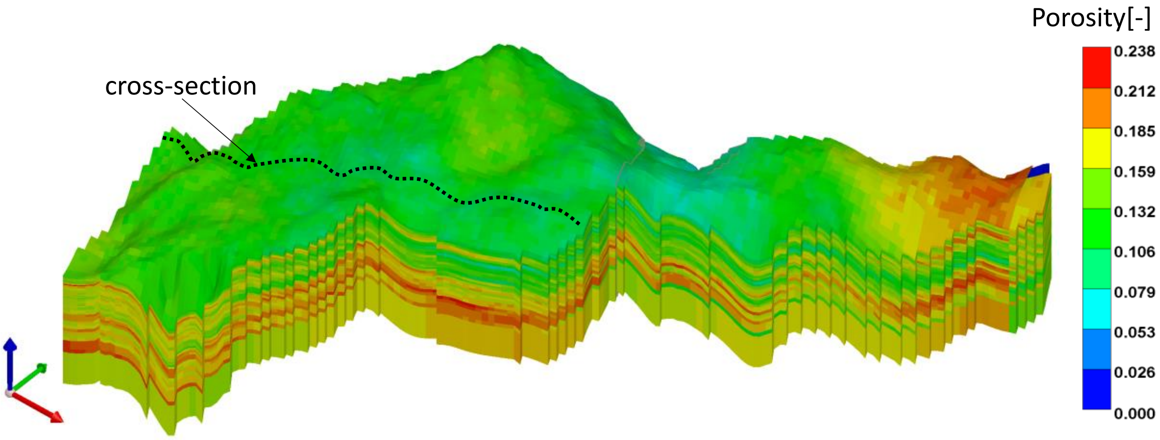

Figure 9. Geological structure of the Viking field, showing the porosity distribution and the location of a vertical cross-section.

The Viking field is an offshore field located within the coast of Lincolnshire in the North Sea, at a depth of approximately 2780m subsea. The reservoir consists of a heterogeneous sandstone formation with an average porosity of about 15% and permeability ranging from 10^{-12} to 10^{-14} m^2 (see Figure 9). The reservoir includes several normal faults with hanging wall blocks.

A vertical cross-section of the reservoir is considered in this study, as shown in Figure 10a. The location of this cross-section, which intercepts a normal fault, is also shown in Figure 9. Impermeable flow condition is used for all the boundaries. We consider supercritical CO_2, which has been injected outside our modeling area, to be trapped under the cap rock within a layer of about 100m thickness (Figure 10a). In this layer, the concentration of CO_2 is considered to be constant ($6\ [\mathrm{mol/m^3}]$). The initial concentration of CO_2 in the bottom layer is assumed to be zero $\left(\left(C_{CO_2}\right)_0 = 0\right)$. No mass transport boundary condition is imposed at the interface between the top and bottom layers. Instead, the full advection-diffusion-dispersion-reaction equation is applied in the bottom layer, while in the top layer; zero-time derivative of the CO_2 concentration is applied. Zero CO_2 flux is imposed at the vertical boundaries and at the bottom surface. The carbonic acid resulting from the dissolution of CO_2 in the host water reacts with Calcium carbonate minerals of the site. Dissolution reaction processes are modeled with the second-order kinetic model, as in equations (15) and (16). The corresponding parameters are given in Table 3 (Sainz-Garcia et al., 2017; Sanjuan and Girard, 1996; Sjöberg and Rickard, 1984). No chemical reaction is considered in the top layer. The initial concentration of $CaCO_3$ in the bottom layer is assumed to be $6\ [\mathrm{mol/m^3}]$. The reservoir is simulated for a duration of 100 years. Dispersion-diffusion processes are considered in the simulation of the field case. Longitudinal and transversal dispersivities are given in table 3.

The reservoir is simulated with the three models described in the previous section ("Isothermal", "Linear temperature" and 'RTHC"). For "Isothermal" the temperature is assumed to be constant (365°[K]). For "Linear temperature" the temperature is invariable in time. It increases linearly with depth. The geothermal gradient is 30° [*K/km*]. The lowest temperature at the higher point of the vertical cross-section is 357.15° [K]. This linear temperature distribution is used as an initial condition in the RTHC model. In this model, the temperature of the injected CO_2 is assumed to be 303.15° [K]. This temperature is applied to the top boundary while the constant geothermal temperature is imposed at the bottom surface. The vertical boundaries are assumed to be adiabatic.

The porosity and permeability maps of the domain are shown in Figures 10b and 10c, respectively (Omar et al., 2021). Temperature-dependent viscosity is considered as in equation (11). All physical properties of rocks and fluid are summarized in Table 3.

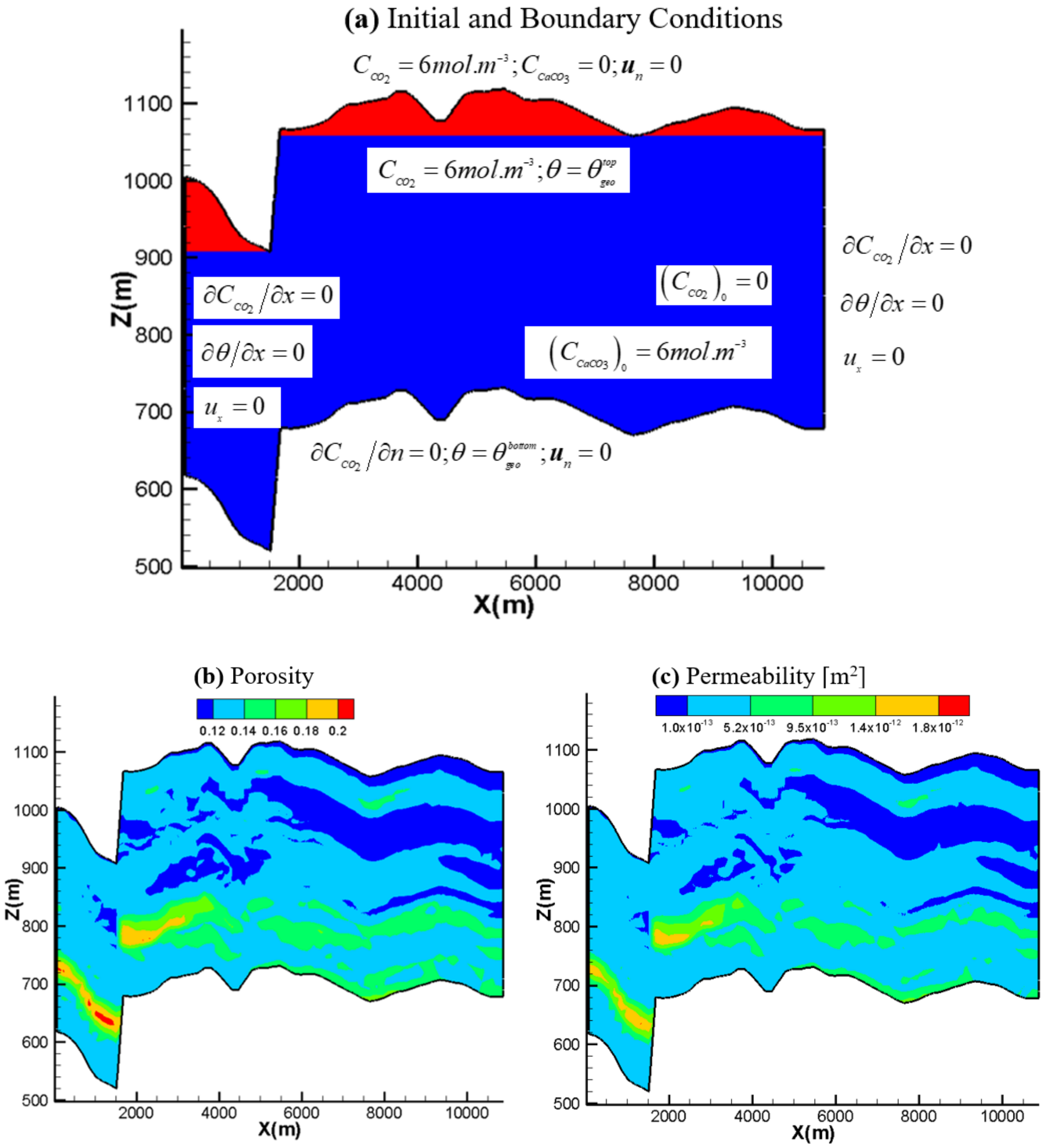

Figure 10. Description of the site: (a) initial and boundary conditions (b) Porosity map, (c) permeability map

Table 3. Physical parameters used for the simulations of the real case

Parameter	***Value***
Gas constant	$R = 8.314 J.mol^{-1}.K^{-1}$
Reference Temperature	$T_{\mathrm{Ref}} = 277.15^{\circ} K$
Freshwater density	$\rho_0 = 1000 \text{ kg.m}^{-3}$
Density of rock	$\rho_R = 2600 \text{ kg.m}^{-3}$
Thermal capacity of water	$CP_f = 4200 \text{ J.kg}^{-1}\text{.K}^{-1}$
Thermal capacity of rock	$CP_R = 880 \text{ J.kg}^{-1}\text{.K}^{-1}$
Thermal Conductivity of water	$\lambda_f = 0.65 \text{ W.m}^{-1}\text{.K}^{-1}$
Thermal Conductivity of rock	$\lambda_R = 3.63 \text{ W.m}^{-1}\text{.K}^{-1}$
Thermal expansion coefficient of water	$\beta_T = 0.001 \text{K}^{-1}$
Mass Expansion	$\beta_C = 0.00833 m^3.mol^{-1}$
Diffusion coefficient of dissolved $\mathrm{CO_2}$	$D_{CO_2} = 5.32 \times 10^{-9} m^2.s^{-1}$
Longitudinal dispersivity	$\alpha_L = 5m$
Transversal dispersivity	$\alpha_T = 0.5m$
Activation energy	$E_a = 20 kJ.mol^{-1}$
Pre-exponential factor	$A = 10^{-8} m^3.mol^{-1}.s^{-1}$

The results of the three models are plotted in Figure 11. This figure depicts the spatial distribution for CO_2 and $CaCO_3$ concentrations and temperature at the end of the simulation (after 100 years). Figure 11 shows that, in contrast to the previous hypothetical benchmark, almost equivalent results are obtained with “Isothermal” and “Linear temperature” models. Figures 11a and 11d show that, with “Isothermal” and “Linear” models, there are almost no fingers in the right part of the domain. Some fingers can be seen in the left part, where high permeability is observed. “RTHC” leads to different results. A fingering phenomenon can be observed everywhere in the domain with the “RTHC” model (Figure 11g). Deeper and more developed fingers can be observed in the left part of the domain, where permeability is relatively high. In general, everywhere in the domain, the fingering phenomenon is more intensive with the “RTHC” than other models. This result gives first evidence that temperature can intensity the fingering phenomenon. This is important for GCS because the fingering phenomenon can affect the processes of CO_2 dissolution. However, these results should be considered with caution, and further simulations should be developed to better understand this behavior. Indeed, in the simulation with the "RTHC" model, the temperature at the top surface is lower than that used in the "Linear temperature" model. This latter is equivalent to the geothermal temperature. Thus, the temperature gradient between the top and bottom surfaces is higher in "RTHC" than in "Linear temperature". This means that the difference between the fingering intensities observed with "RTHC" and "Linear temperature" could not be related to the heat transfer processes that are neglected in "Linear temperature", but rather to the different temperature gradients used in these models. To verify this point, we developed a further simulation with the "RTHC" model, in which we assume that the temperature of CO_2 trapped at the top surface of the reservoir is equivalent to the geothermal temperature in this zone. The results (not shown for the sake of brevity) of this simulation show intensive fingers, which confirms clearly that the intensified fingers with the "RTHC" model are related to the effect of temperature created but the geothermal temperature gradient.

As in the previous example, the total amount of $CaCO_3$ per unit of width ($\Sigma C_{CaCO_3}\left[mol/m\right]$), available in the domain, is also investigated. It is given by:

$$\Sigma C_{CaCO_3} = \iint C_{CO_2} d\Omega \tag{32}$$

The cumulative total flux of CO_2 at the top surface is also investigated. It is given by:

$$TFC_{CO_2}^{Cum} = \int_0^t TFC_{CO_2} dt \tag{33}$$

Where t is the time and TFC_{CO_2} is the instantaneous total flux at the top surface. TFC_{CO_2} is given by:

2

$$TFC_{CO_2} = \oint_{\text{top surface}} \left(u_z C_{CO_2} - \frac{\partial C_{CO_2}}{\partial z} \right) dl \qquad (34)$$

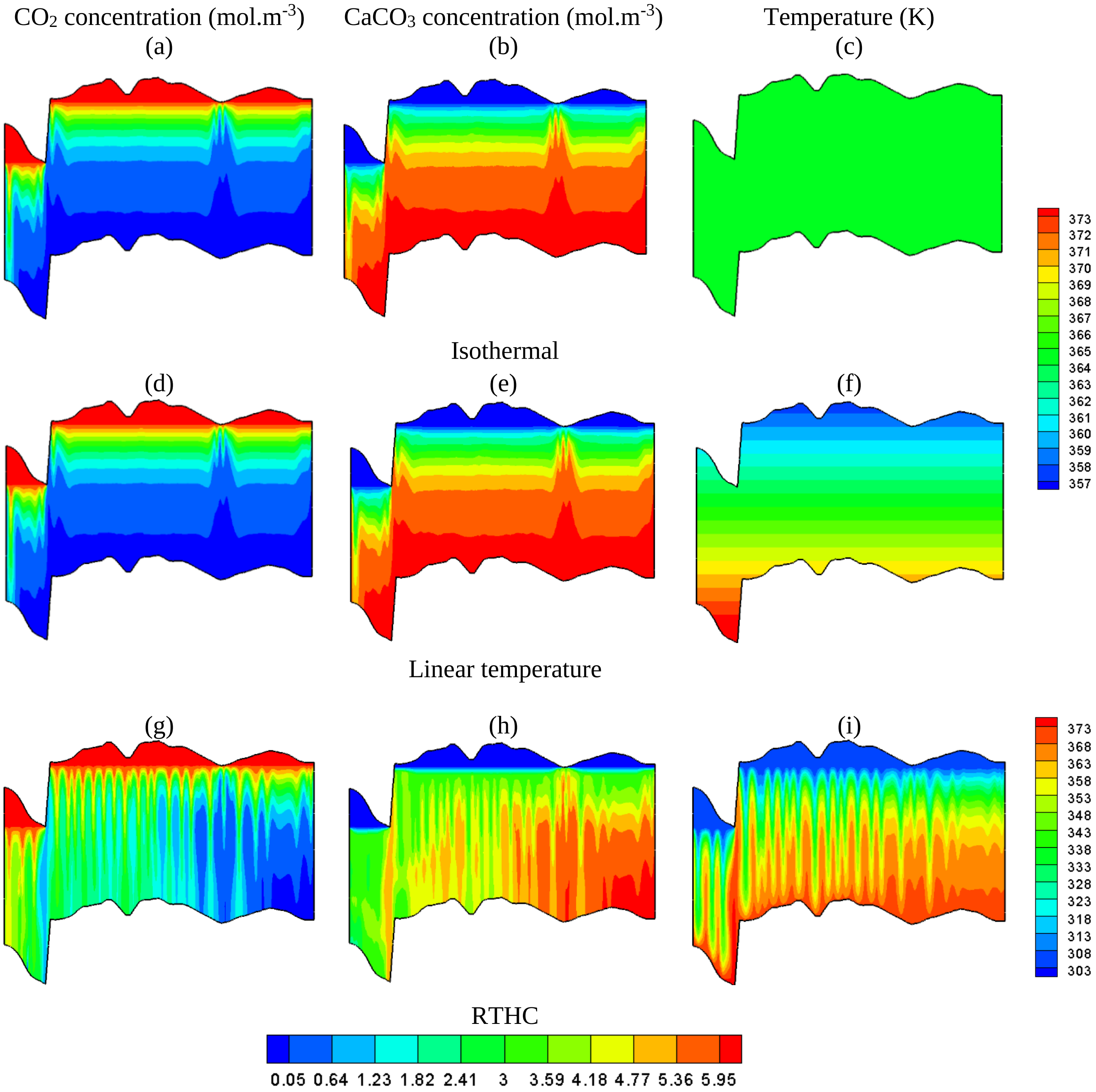

Figure 11. Results of the three models "Isothermal", "Linear temperature" and "RTHC": Spatial distributions of CO_2 (left), $CaCO_3$ (middle), and temperature (right) after 100 years.

The results of the three models regarding the total amount of $CaCO_3$ and cumulative CO_2 flux are given in Figure 12. Equivalent results are obtained with "Isothermal" and "Linear temperature" models, as for the spatial distributions of CO_2, $CaCO_3$, and temperature in Figure

11. Figures 11 and 12 confirm that, when the heat transfer processes are not considered, the effect of temperature variability on the processes of convective-reactive CO_2 dissolution is limited. Figure 12 shows different results with the “RTHC’ model and indicates that heat transfer processes have a significant impact on the dissolution of CO_2 and in consequence, on the total CO_2 flux and the total amount of $CaCO_3$. For the first 20 years, the cumulative total flux of CO_2 is over-predicted with the models “Isothermal” and “Linea temperature” (Figure 12a). This is related to the low temperature of CO_2 trapped below the caprock that can slow down the dissolution processes at the top surface of the reservoir. This is clear in Figure 12b, which shows more dissolution with “Isothermal” and “Linear temperature” models than “RTHC” model. After this first period of 20 years, the heat transfer processes occur due to convection. They increase the temperature in the reservoir and enhance the dissolution processes. The total amount of available $CaCO_3$ becomes over-predicted with the “Isothermal” and “Linear temperature” models. More dissolution leads to more infiltration of trapped CO_2 to the reservoir as it can be observed in Figure 12a. This figure shows that the “Isothermal” and “Linear temperature” models under-predict the cumulative CO_2 flux after 20 years of simulation.

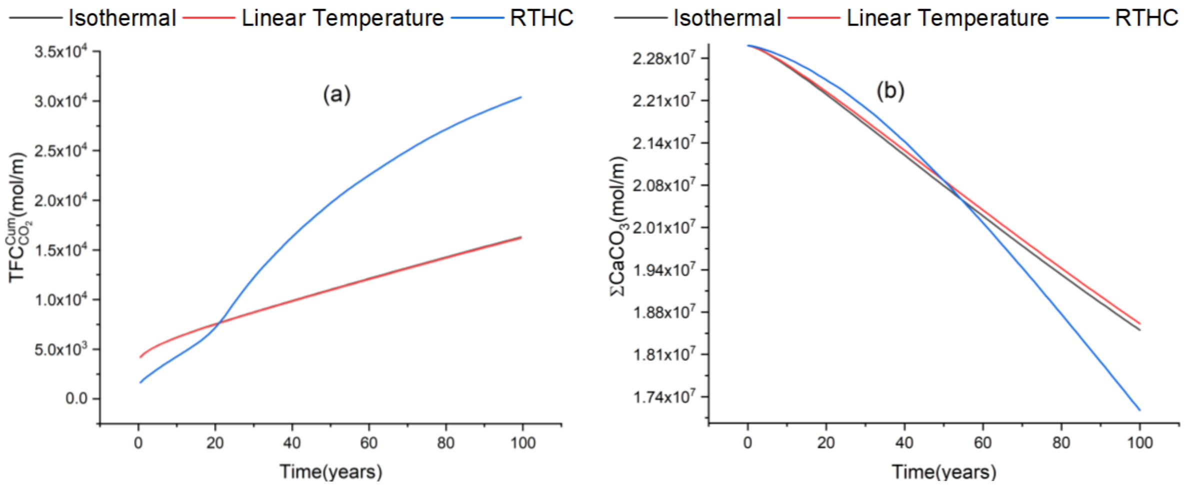

Figure 12. Comparison between models “Isothermal”, “Linear temperature” and “RTHC”: (a) cumulative CO_2 flux and (b) total amount of $CaCO_3$ available in the domain.

The results in the previous analysis are based on deterministic values of parameters. However, several parameters could be uncertain. Thus, it is important to investigate the sensitivity of the results to uncertain parameters. A full sensitivity analysis can be performed in this context. However, as the main goal of this study is to investigate the effect of temperature of dissolution processes on CO_2, we limited the sensitivity analysis to the parameters governing the rate of the dissolution, namely the activation energy (Ea) and the pre-exponential factor (A) in the Arrhenius law. We developed 9 further simulations with the "RTHC" model by considering all combinations of low, moderate and high values of Ea and A. For Ea the low, moderate and high values are considered to be 20, 40 and 60 ($kJ.mol^{-1}$) while these values for A are assumed to be 10^{-6}, 10^{-7} and 10^{-8} ($m^3.mol^{-1}.s^{-1}$).

Figure 13 shows the CO_2 concentration maps resulting from 9 simulations with the RTHC model. It can be observed that increasing the pre-exponential factor intensifies the fingering processes and leads to more CO_2 dissolution. This is also observed when the value of the activation energy is increased from 20 to $40\,kJ.mol^{-1}$. However, almost equivalent results are observed when Ea is increased from 40 to $60\,kJ.mol^{-1}$. Sensitivity of the CO_2 concentration to Ea is less pronounced at a high pre-exponential factor.

2

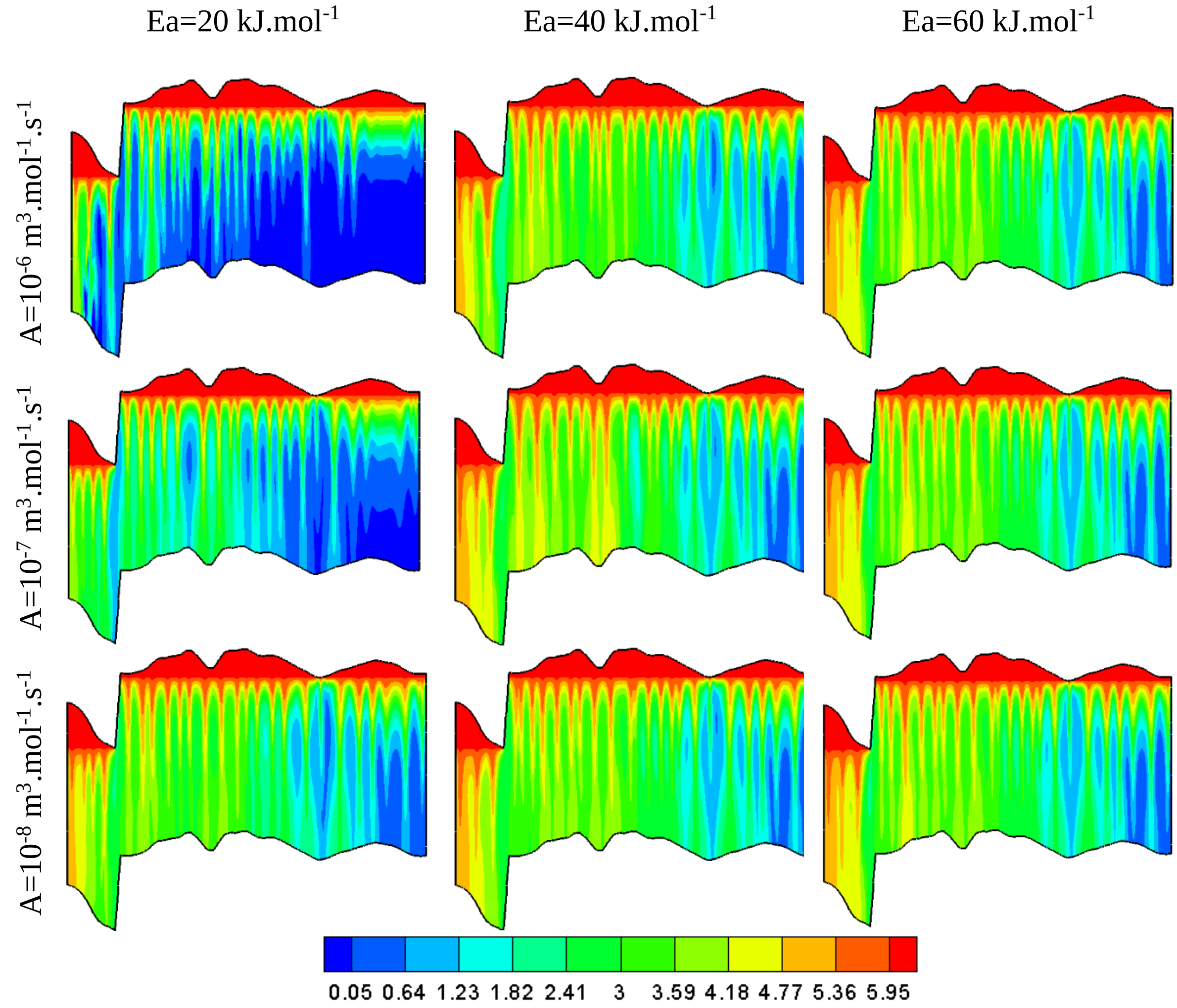

Figure 13. Results of reaction parameters sensitivity analysis with "RTHC" model: Spatial distributions of CO_2

The results of reaction parameters sensitivity analysis regarding the cumulative CO_2 flux $\left(TFC_{CO_2}^{Cum}\right)$ are given in Figure 14. Figures 14a and 14c show that the cumulative CO_2 flux is more sensitive to the activation energy at lower pre-exponential factor. Whatever the value of A, there is no monotonic variation of $TFC_{CO_2}^{Cum}$ with respect to Ea. $TFC_{CO_2}^{Cum}$ is augmenting when Ea is increased from 20 to 40 $kJ.mol^{-1}$, and then it is dropping when Ea is increased from 40 to 60 $kJ.mol^{-1}$. At high value of the pre-exponential factor, equivalent results are obtained for the high and low values of Ea. However, at low values of the pre-exponential factor, the results become different at after 70 years of simulation. Figures 14b and 14d show that the cumulative CO_2 flux is more sensitive to A at high activation energy. No monotonic sensitivity to A can be observed. $TFC_{CO_2}^{Cum}$ is augmenting when A increases from 10^{-6} to 10^{-7} $m^3.mol^{-1}.s^{-1}$ and is weakening when A increases from 10^{-7} to 10^{-8}. Results obtained with A equal to 10^{-6} and 10^{-7} $m^3.mol^{-1}.s^{-1}$ are almost equivalent with the lowest value of activation energy. For the highest value of activation energy, these results become different, and the discrepancy between them increases with time.

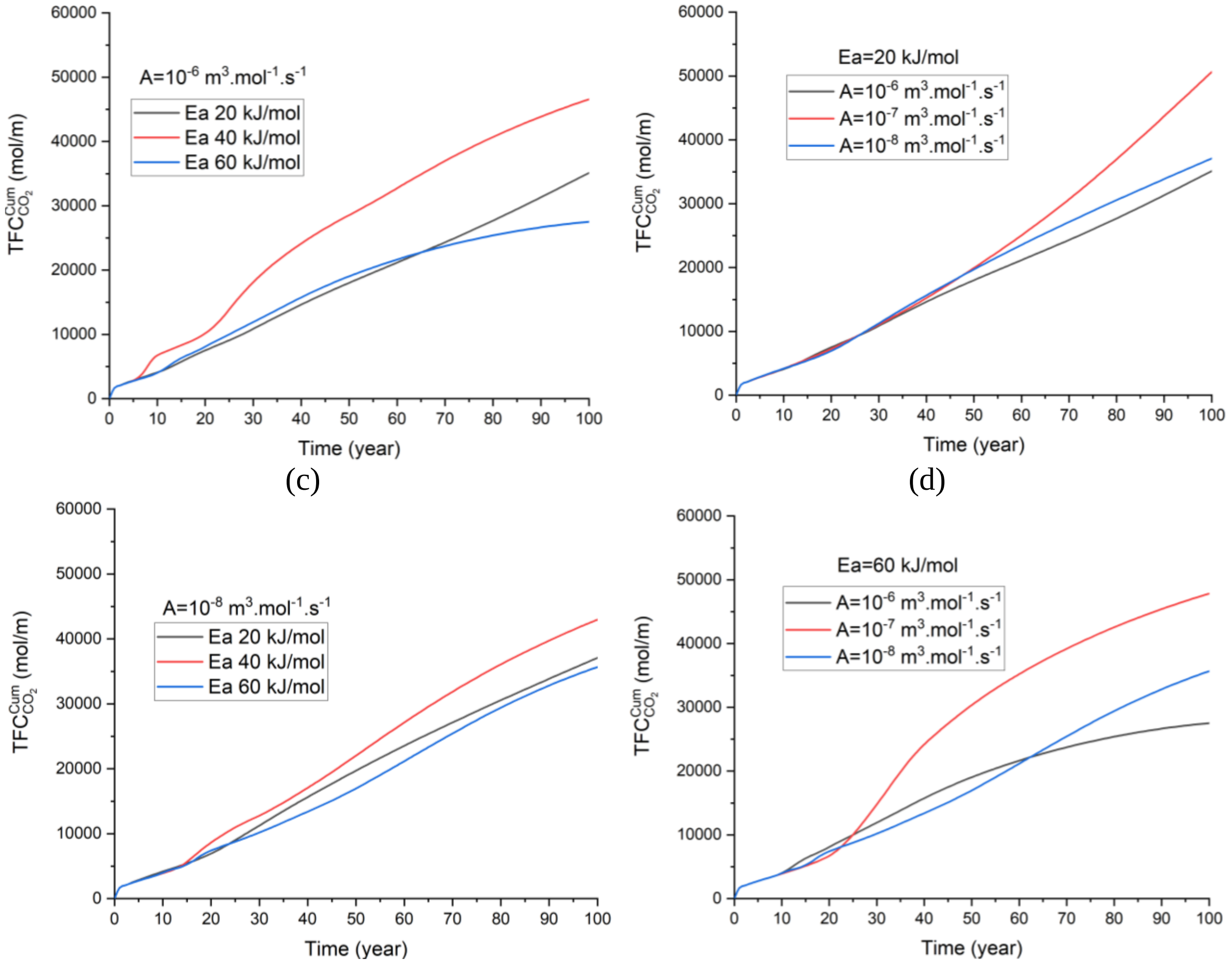
‘Ea’ sensitivity analysis

‘A’ sensitivity analysis

(a)

(b)

(c)

(d)

Figure 14. Comparison between the results of cumulative CO_2 flux with low, moderate and high values of activation energy and pre-exponential factor in the Arrhenius law: (a) and (c): Activation energy sensitivity analysis, (b) and (d): pre-exponential factor sensitivity analysis.

5. Conclusion

Most of previous modeling-based studies on the convective-reactive transport of CO_2 in geological formations are limited to isothermal conditions and deal with small spatial scale problems. The main goal of this work is to investigate the effect of temperature on convective-reactive transport of CO_2 at large field scale. Thus, an advanced numerical model (TRACES) is developed for the simulation of RTHC process in the application of GCS. Appropriate numerical techniques are implemented in TRACES for the discretization of the spatial derivatives (MHFE and DGFE methods) and time integration (error control time stepping). The new model is verified against a standard finite element solution obtained with COMSOL Multiphysics. Good agreement has been obtained for low Rayleigh numbers. The advantages of TRACES are compared with the standard Finite Element solutions, based on the common benchmark of porous box. Results demonstrated that TRACES solutions are less mesh-dependent than the standard Finite element method, especially at high Rayleigh numbers. The DGFE allows for reducing spurious oscillations and for controlling numerical diffusion that can have significant impact on the model accuracy and performance. We provided quantitative data that can be used as reference solutions for benchmarking RTHC models in further studies.

The effects of temperature on the convective-reactive transport of CO_2 are investigated by using three different models with increasing level of complexity: Isothermal, Linear Temperature and RTHC. In “Isothermal” model the temperature is constant while in “Linear Temperature” model the temperature increases linearly with depth. The results of the porous box benchmark indicate that fingering phenomenon is under-predicted when the RTHC processes are neglected. The effect of temperature on CO_2 transport is also investigated for a field case in the Viking reservoir in the North Sea. The results confirm that, at large scale and under realistic conditions of heterogeneity, neglecting the RTHC processes leads to an underestimation of the fingering

$_2$

phenomenon. The results show also that the intensified fingering phenomenon improves the dissolution processes and increase the total flux of CO_2 to the domain.

The parameters controlling the effect of temperature on the reaction rate, namely the activation energy and the pre-exponential factor in the Arrhenius law, are uncertain. A sensitivity analysis is performed to investigate how the uncertainties related to these parameters can affect the results. This analysis shows that the increase of the pre-exponential factor intensifies the fingering processes and leads to more CO_2 dissolution. Sensitivity of the CO_2 concentration to the activation energy is less pronounced at a high pre-exponential factor. The cumulative CO_2 flux is highly sensitive to the activation energy at lower pre-exponential factor. There is no monotonic variation of the total flux with respect to the activation energy. The cumulative CO_2 flux is highly sensitive to the pre-exponential at high activation energy.

References:

Ahmadinia, M., Shariatipour, S.M., Andersen, O., Nobakht, B., 2020. Quantitative evaluation of the joint effect of uncertain parameters in CO2 storage in the Sleipner project, using data-driven models. International Journal of Greenhouse Gas Control 103, 103180. https://doi.org/10.1016/j.ijggc.2020.103180

Andres, J.T.H., Cardoso, S.S.S., 2011. Onset of convection in a porous medium in the presence of chemical reaction. Phys. Rev. E 83, 046312. https://doi.org/10.1103/PhysRevE.83.046312

Babaei, M., Islam, A., 2018. Convective-Reactive CO 2 Dissolution in Aquifers With Mass Transfer With Immobile Water. Water Resour. Res. 54, 9585–9604. https://doi.org/10.1029/2018WR023150

Batlle, F., Carrera, J., Ayora, C., 2002. A comparison of lagrangian and eulerian formulations for reactive transport modelling, in: Developments in Water Science. Elsevier, pp. 571–578. https://doi.org/10.1016/S0167-5648(02)80110-1

Boudreau, B.P., Sulpis, O., Mucci, A., 2020. Control of CaCO3 dissolution at the deep seafloor and its consequences. Geochimica et Cosmochimica Acta 268, 90–106. https://doi.org/10.1016/j.gca.2019.09.037

Chen, Z., Wu, Y.-P., Feng, G.-L., Qian, Z.-H., Sun, G.-Q., 2021. Effects of global warming on pattern dynamics of vegetation: Wuwei in China as a case. Applied Mathematics and Computation 390, 125666. https://doi.org/10.1016/j.amc.2020.125666

Collins, M., Knutti, R., Arblaster, J., Dufresne, J.-L., Fichefet, T., Friedlingstein, P., Gao, X., Gutowski, W.J., Johns, T., Krinner, G., 2013. Long-term climate change: projections, commitments and irreversibility, in: Climate Change 2013-The Physical Science Basis: Contribution of Working Group I to the Fifth Assessment Report of the Intergovernmental Panel on Climate Change. Cambridge University Press, pp. 1029–1136.

Emami-Meybodi, H., Hassanzadeh, H., Green, C.P., Ennis-King, J., 2015. Convective dissolution of CO2 in saline aquifers: Progress in modeling and experiments. International Journal of Greenhouse Gas Control 40, 238–266. https://doi.org/10.1016/j.ijggc.2015.04.003

Erfani, H., Babaei, M., Niasar, V., 2020. Signature of Geochemistry on Density-Driven CO Mixing in Sandstone Aquifers. Water Resour. Res. 56. https://doi.org/10.1029/2019WR026060

Fahs, M., Ataie-Ashtiani, B., Younes, A., Simmons, C.T., Ackerer, P., 2016. The Henry problem: New semianalytical solution for velocity-dependent dispersion: NEW SEMIANALYTICAL SOLUTION FOR HENRY PROBLEM. Water Resour. Res. 52, 7382–7407. https://doi.org/10.1002/2016WR019288

Fahs, M., Carrayrou, J., Younes, A., Ackerer, P., 2008. On the Efficiency of the Direct Substitution Approach for Reactive Transport Problems in Porous Media. Water Air Soil Pollut 193, 299–308. https://doi.org/10.1007/s11270-008-9691-2

Fahs, M., Younes, A., Delay, F., 2009. On the use of large time steps with ELLAM for transport with kinetic reactions over heterogeneous domains. AIChE J. 55, 1121–1126. https://doi.org/10.1002/aic.11727

Farajzadeh, R., Ranganathan, P., Zitha, P.L.J., Bruining, J., 2011. The effect of heterogeneity on the character of density-driven natural convection of CO2 overlying a brine layer. Advances in Water Resources 34, 327–339. https://doi.org/10.1016/j.advwatres.2010.12.012

Ghesmat, K., Hassanzadeh, H., Abedi, J., 2011. The impact of geochemistry on convective mixing in a gravitationally unstable diffusive boundary layer in porous media: CO 2 storage in saline aquifers. J. Fluid Mech. 673, 480–512. https://doi.org/10.1017/S0022112010006282

Ghoshal, P., Kim, M.C., Cardoso, S.S.S., 2017. Reactive–convective dissolution in a porous medium: the storage of carbon dioxide in saline aquifers. Phys. Chem. Chem. Phys. 19, 644–655. https://doi.org/10.1039/C6CP06010B

Hamann, E., Post, V., Kohfahl, C., Prommer, H., Simmons, C.T., 2015. Numerical investigation of coupled density-driven flow and hydrogeochemical processes below playas. Water Resour. Res. 51, 9338–9352. https://doi.org/10.1002/2015WR017833

Hewitt, D.R., Neufeld, J.A., Lister, J.R., 2014. High Rayleigh number convection in a three-dimensional porous medium. J. Fluid Mech. 748, 879–895. https://doi.org/10.1017/jfm.2014.216

Hidalgo, J.J., Carrera, J., 2009. Effect of dispersion on the onset of convection during CO 2 sequestration. J. Fluid Mech. 640, 441–452. https://doi.org/10.1017/S0022112009991480

Hidalgo, J.J., Dentz, M., Cabeza, Y., Carrera, J., 2015. Dissolution patterns and mixing dynamics in unstable reactive flow: MIXING IN UNSTABLE REACTIVE FLOW. Geophys. Res. Lett. 42, 6357–6364. https://doi.org/10.1002/2015GL065036

Hirthe, E.M., Graf, T., 2012. Non-iterative adaptive time-stepping scheme with temporal truncation error control for simulating variable-density flow. Advances in Water Resources 49, 46–55. https://doi.org/10.1016/j.advwatres.2012.07.021

Hoteit, H., Fahs, M., Soltanian, M.R., 2019. Assessment of CO2 Injectivity During Sequestration in Depleted Gas Reservoirs. Geosciences 9, 199. https://doi.org/10.3390/geosciences9050199

Hoteit, H., Firoozabadi, A., 2018. Modeling of multicomponent diffusions and natural convection in unfractured and fractured media by discontinuous Galerkin and mixed methods: Modeling of multicomponent diffusions and natural convection. Int J Numer Methods Eng 114, 535–556. https://doi.org/10.1002/nme.5753

Hoteit, H., Firoozabadi, A., 2008. Numerical modeling of two-phase flow in heterogeneous permeable media with different capillarity pressures. Advances in Water Resources 31, 56–73. https://doi.org/10.1016/j.advwatres.2007.06.006

IPCC. (2019)., n.d.

Islam, A., Korrani, A.K.N., Sepehrnoori, K., Patzek, T., 2014. Effects of geochemical reaction on double diffusive natural convection of CO 2 in brine saturated geothermal reservoir. International Journal of Heat and Mass Transfer 77, 519–528. https://doi.org/10.1016/j.ijheatmasstransfer.2014.05.040

Islam, A.W., Lashgari, H.R., Sephernoori, K., 2014. Double diffusive natural convection of CO2 in a brine saturated geothermal reservoir: Study of non-modal growth of perturbations and heterogeneity effects. Geothermics 51, 325–336. https://doi.org/10.1016/j.geothermics.2014.03.001

Islam, A.W., Sharif, M.A.R., Carlson, E.S., 2013a. Numerical investigation of double diffusive natural convection of CO2 in a brine saturated geothermal reservoir. Geothermics 48, 101–111. https://doi.org/10.1016/j.geothermics.2013.07.001

Islam, A.W., Sharif, M.A.R., Carlson, E.S., 2013b. Numerical investigation of double diffusive natural convection of CO2 in a brine saturated geothermal reservoir. Geothermics 48, 101–111. https://doi.org/10.1016/j.geothermics.2013.07.001

Islam, A.W., Sharif, M.A.R., Carlson, E.S., 2013c. Numerical investigation of double diffusive natural convection of CO2 in a brine saturated geothermal reservoir. Geothermics 48, 101–111. https://doi.org/10.1016/j.geothermics.2013.07.001

Jiang, X., 2011. A review of physical modelling and numerical simulation of long-term geological storage of CO2. Applied Energy 88, 3557–3566. https://doi.org/10.1016/j.apenergy.2011.05.004

Kim, M., Kim, K., Han, W.S., Oh, J., Park, E., 2019. Density-Driven Convection in a Fractured Porous Media: Implications for Geological CO 2 Storage. Water Resour. Res. 55, 5852–5870. https://doi.org/10.1029/2019WR024822

Koohbor, B., Fahs, M., Hoteit, H., Doummar, J., Younes, A., Belfort, B., 2020. An advanced discrete fracture model for variably saturated flow in fractured porous media. Advances in Water Resources 140, 103602. https://doi.org/10.1016/j.advwatres.2020.103602

Lu, C., Han, W.S., Lee, S.-Y., McPherson, B.J., Lichtner, P.C., 2009. Effects of density and mutual solubility of a –brine system on storage in geological formations: “Warm” vs. “cold” formations. Advances in Water Resources 32, 1685–1702. https://doi.org/10.1016/j.advwatres.2009.07.008

Masson-Delmotte, V., Zhai, P., Pörtner, H.-O., Roberts, D., Skea, J., Shukla, P.R., Pirani, A., Moufouma-Okia, W., Péan, C., Pidcock, R., 2018. Global warming of 1.5 C. An IPCC Special Report on the impacts of global warming of 1.

Miller, C.T., Dawson, C.N., Farthing, M.W., Hou, T.Y., Huang, J., Kees, C.E., Kelley, C.T., Langtangen, H.P., 2013. Numerical simulation of water resources problems: Models, methods, and trends. Advances in Water Resources 51, 405–437. https://doi.org/10.1016/j.advwatres.2012.05.008

Moortgat, J., 2017. Adaptive implicit finite element methods for multicomponent compressible flow in heterogeneous and fractured porous media: AIM FOR HETEROGENEOUS FRACTURED MEDIA. Water Resour. Res. 53, 73–92. https://doi.org/10.1002/2016WR019644

Moortgat, J., Amooie, M.A., Soltanian, M.R., 2016. Implicit finite volume and discontinuous Galerkin methods for multicomponent flow in unstructured 3D fractured porous media. Advances in Water Resources 96, 389–404. https://doi.org/10.1016/j.advwatres.2016.08.007

Nordbotten, J.M., Celia, M.A., 2011. Geological Storage of CO2: Modeling Approaches for Large-Scale Simulation. John Wiley & Sons, Inc., Hoboken, NJ, USA. https://doi.org/10.1002/9781118137086

Omar, A., Addassi, M., Vahrenkamp, V., Hoteit, H., 2021. Co-Optimization of CO2 Storage and Enhanced Gas Recovery Using Carbonated Water and Supercritical CO2. Energies 14, 7495. https://doi.org/10.3390/en14227495

Petrou, A.L., 2012. The Free Energy of Activation as the critical factor in geochemical processes. Chemical Geology 308–309, 50–59. https://doi.org/10.1016/j.chemgeo.2012.03.015

Prasad, A., Simmons, C.T., 2005. Using quantitative indicators to evaluate results from variable-density groundwater flow models. Hydrogeol J 13, 905–914. https://doi.org/10.1007/s10040-004-0338-0

Raeisi Isa-Abadi, A., Fontaine, V., Ghafouri, H.-R., Younes, A., Fahs, M., 2020. A fully interior penalty discontinuous Galerkin method for variable density groundwater flow problems. Computers & Fluids 213, 104744. https://doi.org/10.1016/j.compfluid.2020.104744

Rajabi, M.M., Fahs, M., Panjehfouladgaran, A., Ataie-Ashtiani, B., Simmons, C.T., Belfort, B., 2020. Uncertainty quantification and global sensitivity analysis of double-diffusive natural convection in a porous enclosure. International Journal of Heat and Mass Transfer 162, 120291. https://doi.org/10.1016/j.ijheatmasstransfer.2020.120291

Riaz, A., Hesse, M., Tchelepi, H.A., Orr, F.M., 2006. Onset of convection in a gravitationally unstable diffusive boundary layer in porous media. J. Fluid Mech. 548, 87. https://doi.org/10.1017/S0022112005007494

Romanov, V., Soong, Y., Carney, C., Rush, G.E., Nielsen, B., O’Connor, W., 2015. Mineralization of Carbon Dioxide: A Literature Review. ChemBioEng Reviews 2, 231–256. https://doi.org/10.1002/cben.201500002

Sainz-Garcia, A., Abarca, E., Nardi, A., Grandia, F., Oelkers, E.H., 2017. Convective mixing fingers and chemistry interaction in carbon storage. International Journal of Greenhouse Gas Control 58, 52–61. https://doi.org/10.1016/j.ijggc.2016.12.005

Sanjuan, B., Girard, J., 1996. Review of Kinetic Data on Carbonate Mineral Precipitation: BRGM Report R39062. Orléans: BRGM.

Sathaye, K.J., Hesse, M.A., Cassidy, M., Stockli, D.F., 2014. Constraints on the magnitude and rate of CO2 dissolution at Bravo Dome natural gas field. Proceedings of the National Academy of Sciences 111, 15332–15337. https://doi.org/10.1073/pnas.1406076111

Shafabakhsh, P., Ataie-Ashtiani, B., Simmons, C.T., Younes, A., Fahs, M., 2021. Convective-reactive transport of dissolved CO2 in fractured-geological formations. International Journal of Greenhouse Gas Control 109, 103365. https://doi.org/10.1016/j.ijggc.2021.103365

Shao, Q., Fahs, M., Hoteit, H., Carrera, J., Ackerer, P., Younes, A., 2018. A 3-D Semianalytical Solution for Density-Driven Flow in Porous Media. Water Resour. Res. 54. https://doi.org/10.1029/2018WR023583

Shi, X., Chen, J., Gu, L., Xu, C.-Y., Chen, H., Zhang, L., 2020. Impacts and socioeconomic exposures of global extreme precipitation events in 1.5 and 2.0 °C warmer climates. Science of The Total Environment 142665. https://doi.org/10.1016/j.scitotenv.2020.142665

Sigfusson, B., Gislason, S.R., Matter, J.M., Stute, M., Gunnlaugsson, E., Gunnarsson, I., Aradottir, E.S., Sigurdardottir, H., Mesfin, K., Alfredsson, H.A., 2015. Solving the carbon-dioxide buoyancy challenge: The design and field testing of a dissolved CO2 injection system. International Journal of Greenhouse Gas Control 37, 213–219.

Singh, H., Islam, A., 2018. Enhanced safety of geologic CO2 storage with nanoparticles. International Journal of Heat and Mass Transfer 121, 463–476. https://doi.org/10.1016/j.ijheatmasstransfer.2017.12.152

Sjöberg, E.L., Rickard, D.T., 1984. Temperature dependence of calcite dissolution kinetics between 1 and 62°C at pH 2.7 to 8.4 in aqueous solutions. Geochimica et Cosmochimica Acta 48, 485–493. https://doi.org/10.1016/0016-7037(84)90276-X

Soltanian, M.R., Amooie, M.A., Gershenzon, N., Dai, Z., Ritzi, R., Xiong, F., Cole, D., Moortgat, J., 2017. Dissolution Trapping of Carbon Dioxide in Heterogeneous Aquifers. Environ. Sci. Technol. 51, 7732–7741. https://doi.org/10.1021/acs.est.7b01540

Soltanian, M.R., Hajirezaie, S., Hosseini, S.A., Dashtian, H., Amooie, M.A., Meyal, A., Ershadnia, R., Ampomah, W., Islam, A., Zhang, X., 2019. Multicomponent reactive transport of carbon dioxide in fluvial heterogeneous aquifers. Journal of Natural Gas Science and Engineering 65, 212–223. https://doi.org/10.1016/j.jngse.2019.03.011

Tabrizinejadas, S., Fahs, M., Ataie-Ashtiani, B., Simmons, C.T., Chiara Roupert, R., Younes, A., 2020. A Fourier Series Solution for Transient Three-Dimensional Thermohaline Convection in Porous Enclosures. Water Resour. Res. 56. https://doi.org/10.1029/2020WR028111

UNFCCC, D., 2015. 1/CP. 21, Adoption of the Paris Agreement. UN Doc. FCCC/CP/2015/10/Add. 1.

van Reeuwijk, M., Mathias, S.A., Simmons, C.T., Ward, J.D., 2009. Insights from a pseudospectral approach to the Elder problem: PSEUDOSPECTRAL APPROACH TO THE ELDER PROBLEM. Water Resour. Res. 45. https://doi.org/10.1029/2008WR007421

Voss, C.I., Simmons, C.T., Robinson, N.I., 2010. Three-dimensional benchmark for variable-density flow and transport simulation: matching semi-analytic stability modes for steady unstable convection in an inclined porous box. Hydrogeol J 18, 5–23. https://doi.org/10.1007/s10040-009-0556-6

Wang, X., Yang, Y., Dong, Z., Zhang, C., 2009. Responses of dune activity and desertification in China to global warming in the twenty-first century. Global and Planetary Change 67, 167–185. https://doi.org/10.1016/j.gloplacha.2009.02.004

Whitley, S., 2018. G7 fossil fuel subsidy scorecard: Tracking the phase-out of fiscal support and public finance for oil, gas and coal. International Institute for Sustainable Development.

Wu, Y., Li, P., 2020. The potential of coupled carbon storage and geothermal extraction in a CO2-enhanced geothermal system: a review. Geotherm Energy 8, 19. https://doi.org/10.1186/s40517-020-00173-w

Xie, Y., Simmons, C.T., Werner, A.D., Diersch, H.-J.G., 2012. Prediction and uncertainty of free convection phenomena in porous media: PREDICTION OF FREE CONVECTION PHENOMENA IN POROUS MEDIA. Water Resour. Res. 48. https://doi.org/10.1029/2011WR011346

Xu, R., Li, R., Ma, J., He, D., Jiang, P., 2017. Effect of mineral dissolution/precipitation and CO2 exsolution on CO2 transport in geological carbon storage. Accounts of chemical research 50, 2056–2066.

Younes, A., Ackerer, P., 2010. Empirical versus time stepping with embedded error control for density-driven flow in porous media: TIME STEP MANAGEMENT FOR DENSITY-DRIVEN FLOW. Water Resour. Res. 46. https://doi.org/10.1029/2009WR008229

Younes, A., Ackerer, P., Delay, F., 2010. Mixed finite elements for solving 2-D diffusion-type equations. Rev. Geophys. 48, RG1004. https://doi.org/10.1029/2008RG000277

Younes, A., Fahs, M., Ahmed, S., 2009. Solving density driven flow problems with efficient spatial discretizations and higher-order time integration methods. Advances in Water Resources 32, 340–352. https://doi.org/10.1016/j.advwatres.2008.11.003

Younes, A., Fahs, M., Belfort, B., 2013. Monotonicity of the cell-centred triangular MPFA method for saturated and unsaturated flow in heterogeneous porous media. Journal of Hydrology 504, 132–141. https://doi.org/10.1016/j.jhydrol.2013.09.041

Zhang, D., Song, J., 2014. Mechanisms for Geological Carbon Sequestration. Procedia IUTAM 10, 319–327. https://doi.org/10.1016/j.piutam.2014.01.027

Zhang, Z., Huisingh, D., 2017. Carbon dioxide storage schemes: technology, assessment and deployment. Journal of Cleaner Production 142, 1055–1064.